Università degli Studi di Padova

Dipartimento di Ingegneria Civile, Edile e Ambientale
(ICEA)

Tesi di Laurea Magistrale
in Ingegneria Civile

EXPERIMENTAL INVESTIGATION ON PLUG FLOW PHENOMENON INDUCED BY WAVES

INDAGINE SPERIMENTALE SUL FENOMENO
DEL PLUG FLOW INDOTTO DA ONDE

Relatori: Prof.Ing. Piero Ruol

Prof.Ing. Luca Martinelli

Prof. Eric Barthélemi

Laureanda: Giulia Marin

ANNO ACCADEMICO 2014 - 2015

« Considerate la vostra semenza:

fatti non foste a viver come bruti,

ma per seguir virtute e canoscenza. »

vv 119-120

(Dante Alighieri, Inferno XXVI)

Abstract

THE CONDITIONS under which plug formation may occur in oscillatory flow over beds of sediment were examined. The term plug formation is used to describe the situation where sediment starts to move as a solid block when the flow reverses.

In particular they were conducted two experiments, which the second of them has the aim to focus on the enlargement of the area of study of the first experiment to better observe the phenomenon of plug flow. They were conducted in a wave flume using granular sediments of Plexiglas with d50 equal to 0.64mm. The analysis technique chosen is the PIV (Particle Images Velocimetry) and the algorithm to decrypt data was provided by the program UVMAT developed by the laboratory LEGI Grenoble.

In this study was addressed first of all the analysis of phenomena in a global scale, studying the velocity along the vertical and in the time in different bottom depth. Then the results were compared with those found by Zala-Flores and Sleath and were highlighted features in common. It was subsequently studied the second experiment on a local scale to identify the characteristics of the formation of the phenomenon of plug flow. Unsuccessful it has been applied the model of Sleath to locate the shear stress that determines the plug flow. But it has been found finally an optimal method to detect the instants at which it forms the plug flow and a way to know

the approximate local erosion that causes.

Riassunto

SONO STATE esaminate le condizioni in cui può verificarsi la formazione del plug flow durante il flusso oscillatorio sopra il letto di sedimenti. Il termine "plug flow formation" è usato per descrivere la situazione in cui i sedimenti iniziano a muoversi come un blocco solido quando il flusso della corrente si inverte.

In particolare sono stati condotti due esperimenti, di cui il secondo ha lo scopo di focalizzarsi sull'ingrandimento della zona di studio del primo esperimento per meglio osservare il fenomeno del plug flow. Sono stati svolti in un canale artificiale utilizzando sedimenti granulari di plexiglass di d50 pari a 0.64mm. La tecnica di analisi prescelta è quella del PIV (Particle Images Velocimetry) e l'algoritmo per decifrare i dati è fornito dal programma UVMAT sviluppato dal laboratorio LEGI di Grenoble.

In questo studio è stata affrontata prima di tutto l'analisi dei fenomeni in scala globale, studiando la velocità lungo la verticale e nel tempo in diverse profondità del fondale. Quindi i risultati sono stati confrontati con quelli trovati da Zala-Flores e Sleath e si sono evidenziate le caratteristiche in comune. Successivamente si è studiato il secondo esperimento a scala locale per individuare le caratteristiche della formazione del fenomeno del plug flow. Senza successo si è applicato il modello di Sleath per individuare lo sforzo di taglio che determina il plug flow. Ma si è trovato infine un metodo

ottimale per individuare gli istanti in cui si forma il plug flow e un modo approssimativo per conoscere l'erosione locale che provoca.

Acknowledgment

I WISH TO THANK all those who helped me in the writing of the thesis with suggestions, criticisms and comments: to them goes my gratitude, but to me the responsibility for any error contained in this thesis.

I first thank Prof Piero Ruol and Prof Luca Martinelli, Relators, for their many and useful tips that have allowed the realization of this thesis.

I thank Professor Eric Barthélémi, Relator, who welcomed me in the laboratory LEGI in Grenoble and followed me with great patience during my research.

Thanks also to Prof. Hervé Michallet, for his availability to clarify my doubts, and all the employees of the laboratory who helped me during my period of study in Grenoble.

Special thanks to my boyfriend Francesco for his patience and the constant help in the layout I will always be grateful.

I would also like to thank my family that this work is dedicated.

Ringraziamenti

DESIDERO ringraziare tutti coloro che mi hanno aiutato nella stesura della tesi con suggerimenti, critiche ed osservazioni: a loro va la mia gratitudine, anche se a me spetta la responsabilità per ogni errore contenuto in questa tesi.

Ringrazio anzitutto il Prof Piero Ruol ed il Prof Luca Martinelli, Relatori, per i loro molteplici e utili consigli che hanno permesso la realizzazione di questa tesi.

Ringrazio il Professor Eric Barthélemi, Relatore, che mi ha accolto nel laboratorio LEGI di Grenoble e mi ha seguito con tanta pazienza durante la mia ricerca.
Grazie anche al Prof. Hervé Michallet, per la sua disponibilità nel chiarire i miei dubbi, e a tutti i collaboratori del laboratorio che mi hanno aiutata durante il mio soggiorno di studio a Grenoble.

Un particolare ringraziamento va al mio fidanzato Francesco: per la sua pazienza e il costante aiuto nell'impaginazione gli sarò sempre riconoscente.

Vorrei infine ringraziare la mia famiglia a cui questo lavoro è dedicato.

Contents

List of Figures

List of Tables

Chapter 1

State of Art

THE WAY in which sand is moved by the action of water waves is of great practical and scientific importance but is still not fully understood. One area of particular interest is that of sheet flow. When only small amounts of sediment are in motion, the bed is usually covered with ripples or dunes. As the sediment transport rate increases, the height-to-length ratio of the bed forms tends to decrease, and eventually, at very high sediment transport rates, the bed becomes plane. This condition is called sheet flow and it is important because large amounts of sediment are moved by the flow, and consequently, serious erosion or sedimentation may occur in a relatively short time. It is also of interest from the practical point of view because the fact that the bed is plane makes the flow easier to analyse than when the bed is rippled. Because most of the transport occurs within the sheet flow layer, the thickness of this layer is an important parameter. The sheet flow layer thickness is closely related to the erosion depth. Zala Flores and Sleath [1998] found that the erosion depth depends both on the Shields parameter and on the parameter $S = \rho U_0 \omega / (\rho_s - \rho) g$, which represents the ratio of inertial to gravity forces acting on individual grains of sediment.

Here U_0 is the amplitude of the oscillatory velocity just above the boundary layer at the bed; ω is angular frequency; ρ_s and ρ are the dry density of the sediment and the density of the fluid, respectively; and g is the acceleration due to gravity. Sleath [1994] suggested that there are two distinct regimes in oscillatory sheet flow; at low values of the parameter S the mobile layer of sediment behaves as if the flow is quasi-steady, whereas at high values of the parameter S the flow is dominated by the pressure gradient and inertia forces. Traditionally, the incipient motion and near bed transport of sediment is parameterized with the Shields parameter [Shields, 1936], which represents the ratio of the mobilizing force applied by the shear stress over a single layer of grains to the stabilizing force applied by gravity. At the critical limit, the Shields parameter represents the vertical gradient of the shear stress applied over a single grain thickness. Transport models assume incipient motion occurs when some critical bed stress is exceeded (Shields $> 0.03 - 0.06$) and parameterize the sediment concentration as a function of the excess stress [Engelund and Fredsøe, 1976; Zyserman and Fredsøe, 1994; Hanes and Bowen, 1985]. As stress increases, ripples develop and sediment is easily suspended. As stress further increases (Shields $> 0.8 - 1.0$), ripples are washed out and a sheet flow, approximately 10-60 grain diameters of thickness, develops.

It is important to know more about these sediment transport processes since they could have significant implications to improve models of sediments transport or calculate quantities such as the maximum depth of erosion. However, Zala Flores & Sleath have described experiments in which sediments started to move as a solid block when the flow reverses, and this phenomenon is called *plug flow*. Foster(2006) told that the velocity and sediment observations show that, under large pressure gradients present during

the strengthening of onshore directed flow, several centimeters of previously still sediment can be mobilized and transported onshore. These observations are inconsistent with traditional sediment transport theories (Shields, 1936; Bagnold, 1966) that assume incipient motion is only based on the force applied by bed stress but are consistent with theories that include an additional force induced by the horizontal pressure gradient (Sleath, 1999). Recent laboratory and theoretical investigations indicate that when the wave acceleration is large, the bed may temporarily dilate resulting in a significantly larger (O(cm)) mobile bed layer [Sleath, 1999]. In a series of oscillatory laboratory tunnel experiments, bed dilation occurred when the horizontal pressure gradient applied to individual sediment grains dominates the immersed weight of the grains [Dick and Sleath, 1991; Sleath, 1994; Zala Flores and Sleath, 1998]. The horizontal pressure gradient for sinusoidal waves is $\partial p/\partial x = \rho U_0 \omega \sin(\omega t)$, where ω is the angular wave frequency and U_0 is the velocity amplitude. Sleath [1999] characterized the role of the pressure gradient in incipient motion with a ratio between the destabilizing force applied by the peak horizontal pressure gradient to the stabilizing force applied by gravity. Unlike the Shields parameter, the Sleath parameter has no dependence on the grain size. The laboratory observations indicate that plug flow occurs when the Sleath parameter exceeds a critical value of 0.29-0.35. However, in the field it remains very difficult to perform detailed measurements within the dense mobile sediment layer close to the seabed.

The aims of this thesis are to analyse the sheet flow and then to understand the physic phenomena that happens in it, like the plug flow formation. First of all, it was analyzed the characteristics of the experiment in a global scale and it was determined:

- Velocity profiles along vertical direction;
- Statistic propriety as skewness, mean, deviation;
- Interface between still particles and motion particles;
- S number and condition for plug formation to compare them with results found by Sleath (1999);
- Time series of horizontal velocity U in different depth of bed to compare them with results found by Zala-Flores (1998).

Successively it was studied the experiment in a local scale focusing the bed layers. It was chosen a section of image and then it was individuated the formation of plug flow on time. So it was examined the conditions of formation of plug flow using the parameter S number and it was calculated an approximate thickness of some plug flow, in way to insert these information in the model of Sleath and so to make a comparison between shear stress calculated by the model and by the definition $\tau = -\rho\tilde{u}\tilde{v}$.

Noteworthy, it is the kind of technique used to perform the experiments, as it is a very versatile technique used in many areas of science, engineering, and health sciences but are often not well understood. The complex nature of flows may be studied using particle image velocimetry (PIV), a laser based imaging technique for optically accessible flows. Though many forms of PIV exist that extend the technique beyond the original planar two component velocity measurement capabilities, the basic PIV system consists of a light source (laser), a camera, tracer particles, and analysis algorithms. The imaging and recording parameters, the light source, and the algorithms are adjusted to optimize the recording for the flow of interest and obtain valid velocity data. Common PIV investigations measure

two component velocities in a plane at a few frames per second. However, recent developments in instrumentation have facilitated high frame rate ($> 1kHz$) measurements capable of resolving transient flows with high temporal resolution. Therefore, high frame rate measurements have enabled investigations on the evolution of the structure and dynamics of highly transient flows. These investigations play a critical role in understanding the fundamental physics of complex flows.

Chapter 2

Theoretical background

BEFORE addressing the data analysis of the experiments carried out it is good to report the theoretical treatment to which reference was made.They have been studied many scientific papers and some of them were considered to be of considerable importance for the study of the phenomenon of plug flow.

First, we must study the characteristics of velocity and then reference is made as explained by Nielsen (1992).

Then we study the dynamics of the formation of plug flow examined by Sleath (1999) who formulated also a model to determine shear stress required to start the plug flow.

Finally, it describes the way to determine the thickness of the sheet flow that is the area in which it presents the phenomenon of plug flow.

2.1 Profile of horizontal velocity U along vertical (Nielsen 1992)

THE WAVE boundary layer is intuitively defined as the layer close to the bottom, where the wave induced by water motion is noticeable affected by the boundary. This layer is normally very thin, generally a few millimeters over a smooth, solid bed and a few centimeters over a flat bed of loose sand. Although the water motion induced by natural waves is not simple harmonic, it is instructive and useful to study the simple harmonic, oscillatory boundary layer, which corresponds to $u_\infty = A\omega\cos(\omega t)$ and use it as an approximation to natural wave boundary layers.

The total picture of the velocity variation in such a layer is at first sight very complicated because both amplitude and relative phase change with the distances from the bed. In the Figure 2.1 it can be seen the velocity profile along vertical. Note that the velocity near the bed turns before the free stream velocity and that the velocity amplitude is largest in a zone near the bottom, not a z corresponding free stream. Indeed, another typical feature of oscillatory boundary layers is the "overshoot" near the bed and this happens when there are elevations where the velocity amplitude U exceeds Aω.

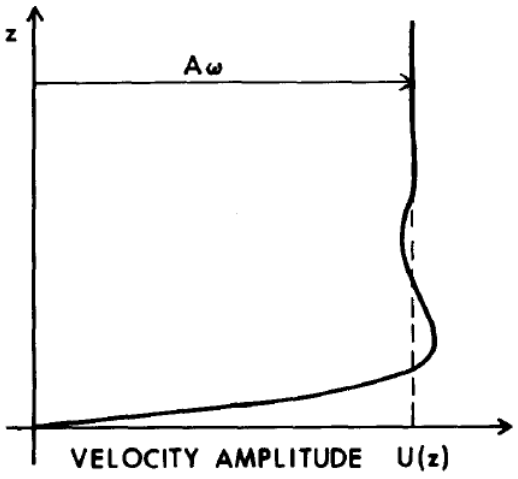

Figure 2.1. Local velocity amplitude U(z)

2.2 Dynamics for plug flow formation and Sleath model (1999)

SLEATH EXAMINED the conditions under which plug flow formation may occur in oscillatory flow over beds of sediment. The term plug flow is used to describe the situation where sediment starts to move as a solid block when the flow reverses. It is shown analytically that there is a lower bound on the value of the parameter S for plug flow formation. For values of S above this limit plug flow formation is determined by the degree of compaction of the sediment. Sleath considered the equilibrium of the shaded volume of sediment shown in Figure 2.2.

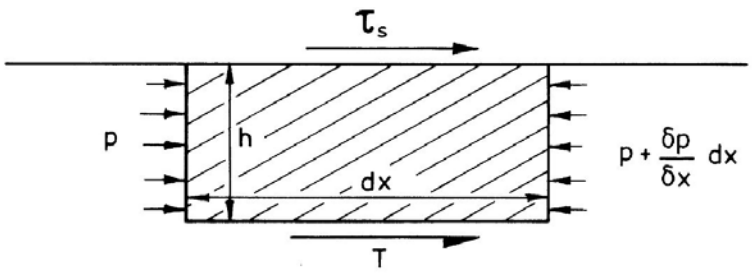

Figure 2.2. Forces on a section of bed

The volume of sediment is of length dx, depth h, and thickness unity into the page. On the upper surface a shear stress τ_s is exerted by the flow. On the lower surface there is a shear stress due to the resistance of the bed below. The pressure is p and x is the distance measured horizontally. We assume that the length of the waves producing the flow is very large compared with h and we consider the situation where the shaded volume is just starting to slide horizontally. The motion of a block of sediment after a period of crest may require upward movement of the block due to dilatation in the slip layer as particles, which previously rested in hollows between grains, are pushed up over crests. Suppose that the shaded volume is pushed up a distance αD in time t^* where α is a constant and D is the median grain diameter. If sediment is pushed up water must move down.

Thus, the mean downward percolation velocity of water through sediment is $\alpha D/t^*$. If Darcy's law applies the vertical pressure gradient due to this percolation is:

$$\frac{\partial p}{\partial z} = \frac{\mu \alpha D}{K_s t^*} \tag{2.1}$$

where μ is the dynamic viscosity, K_s is the specific permeability and z is the distance measured vertically. If there is no sediment in the flow above, the weight of sediment carried by the grains at the bottom of the shaded volume will be $(\rho_s - \rho)ghC^*$ where ρ_s and ρ are the density of the sediment and the fluid, respectively, C^* is the concentration of the sediment and g is the acceleration due to gravity. Thus, making use the precedent equation, the vertical component of stress carried by grain/grain interactions at the lower surface of the shaded volume is:

$$P = (\rho_s - \rho)ghC^* + \left(\frac{\mu \alpha D}{K_s t^*}\right)h \tag{2.2}$$

For the test conditions of Zala-Flores & Sleath acceleration terms in the equations for the flow in the porous bed are negligible. Thus, at the instant when the plug flow of sediment is just about to move

$$Tdx = h\frac{\partial p}{\partial x}dx - \tau_s dx \tag{2.3}$$

Since there is no sudden change in flow conditions or bed friction, the initial acceleration of the plug flow is negligibly small. Consequently, this equation will continue to apply just after the plug flow has started to move.

By analyzing the experiments, it is deduced that $\partial p/\partial x$ in the seabed is the forcing of the system, since, due to the phase delay, is very high compared to the situation of the fluid above it. So to balance the system, it creates a sudden movement of the grains of the seabed and this phenomenon

is the plug flow.

As it will see below, the number S can also be defined by $\partial p/\partial x$ and then use this dimensionless number to study the phenomenon is a good criterion.

Following Bagnold (1956), we assume that for non-cohesive sediment $|T| = KP$ where K is the dynamic equivalent of the static coefficient of friction. Substituting all these equations into the last equation, we obtain

$$\left|\frac{\partial p}{\partial x} - \frac{\tau_s}{h}\right| = KC^*(\rho_s - \rho)g + K\frac{\partial p}{\partial z} \tag{2.4}$$

If the horizontal velocity in the free stream flow is $u = U_0 \cos(\omega t)$ it follows that

$$\left|\frac{\partial p}{\partial x}\right| = \rho U_0 \omega \sin(\omega t) \tag{2.5}$$

And defining Sleath number as

$$S = \frac{-\frac{\partial u_\infty}{\partial t} \cdot \rho}{(\rho_s - \rho)g} = \frac{\frac{\partial p}{\partial x}}{(\rho_s - \rho)g} \tag{2.6}$$

The big equation becomes

$$\left|S\sin(\omega t) - \frac{\tau_s}{(\rho_s - \rho)gh}\right| = KC^*\left(1 + \frac{\frac{\partial p}{\partial z}}{(\rho_s - \rho)g}\right) \tag{2.7}$$

The limit condition is when $|S| \approx KC^*$ and Sleath (1998) determined that this value is usually around 0.35 for his experiments.

2.3 Sleath model in detail

THE CONDITIONS for the movement indicate that if the shear stress at the interface between sediment and fluid plus the strength of volume due to the pressure gradient exceeds the basement constraint R_T then a plug flow starts moving. This result is in the expression:

$$\left|\tau - \delta_s \frac{\partial p}{\partial x}\right| \geq R_T \tag{2.8}$$

with:

- $R_T = K_f P$;
- P is the resultant of the vertical forces that are applied to the mix of grains and fluid and is called apparent weight:

$$\begin{aligned} P &= C^*(\rho_s - \rho)g\delta_s + p(z=0) - p(z=-\delta_s) \\ &\cong \delta_s\left(C^*(\rho_s - \rho)g + \frac{\partial p'}{\partial z}(z=0)\right) \end{aligned} \tag{2.9}$$

The parameter p' is the excess pore pressure, $(p - \rho g z)$, because the hydrostatic component (Archimedes force) is already in the apparent weight $C^*(\rho_s - \rho)g\delta_s$. If this expression is checked in a block is set in motion. Can be rewritten with dimensionless numbers:

$$\left|\frac{d_{50}}{\delta_s}\theta - S\right| \geq K_f\left(C^* + \frac{1}{g\Delta\rho}\frac{\partial p'}{\partial z}(z=0)\right) \tag{2.10}$$

It was a new condition for moving that recognizes the vertical pressure gradient, which reduces or increases the block linked to ex-filtration /in-filtration (but without making Darcy hypothesis). If these conditions are satisfied, then the balance of forces of the sediment block (plug) (according to the signs of the forces of Figure 2.3) can be written:

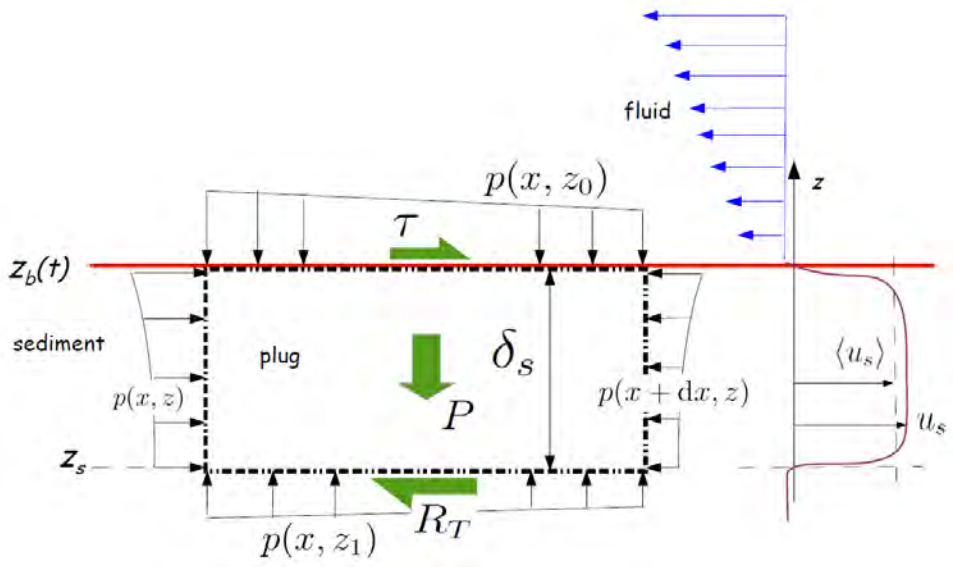

Figure 2.3. Dynamics forces in plug flow

$$\rho_m \int_{z_b(t)}^{z_s(t)} \frac{\partial u_s}{\partial t} dz = -\delta_s \frac{\partial p}{\partial x} + \tau - R_T$$

$$\longrightarrow \rho_m \delta_s \frac{\partial \langle u_s \rangle}{\partial t} - \rho_m \langle u_s \rangle \frac{\partial z_s}{\partial t} = -\delta_s \frac{\partial p}{\partial x} + \tau - R_T$$

with u_s skating speed and R_T which is calculated by bringing the weight P apparent, or resulting vertical forces, and $\delta_s = z_s - z_b$.

It is assumed that there is not vertical acceleration, so the shear stress is:

$$\tau = \delta_s \left[K_f C^* (\rho_s - \rho) g + K_f \frac{\partial p'}{\partial z} + \rho_m \frac{\partial \langle u_s \rangle}{\partial t} - \rho_m \frac{\langle u_s \rangle}{\delta_s} \frac{dz_s}{dt} + \frac{\partial p}{\partial x} \right] \quad (2.11)$$

It was calculated the shear stress with this formula and it was compared with the shear stress considered as $\tau = -\rho \tilde{u} \tilde{v}$.

2.4 Thickness of Sheet flow

One area of particular interest is that of sheet flow. When only small amounts of sediment are in motion, the bed is usually covered with ripples or dunes. As the sediment transport rate increases, the H/L of the bed forms tends to decrease, and eventually, at very high sediment transport rates, the bed becomes plane.

This sheet flow condition is important because large amounts of sediment are moved by the flow, and consequently, serious erosion or sedimentation may occur in a relatively short time. It was defined the thickness of the sheet flow, distance between the bottom interface, which identifies the layer of separation between the particles in motion and static particles, and the upper interface, which separates the region of the particles very concentrated from the one where the particles are little concentrated (Figure 2.4). Unfortunately, the concept of concentration is relative, because in the experiment it wasn't measured, but through other expedients later it will come to calculate.

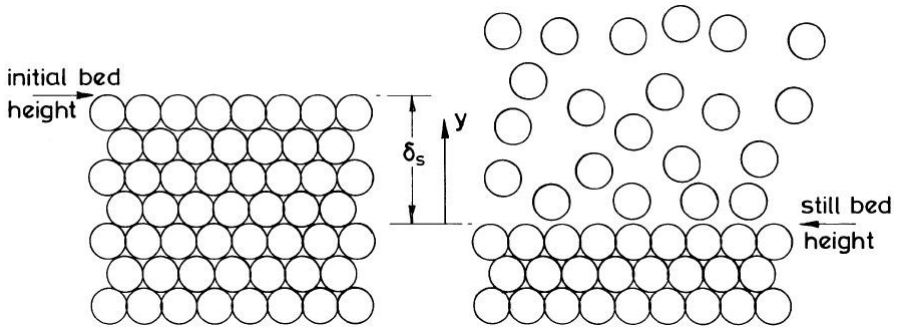

Figure 2.4. Reference system for the initial bed height

Chapter 3

Methods, experiments setup & measurements

THIS CHAPTER explains the ways in which the experiments were conducted, measurement techniques, the instrument for data analysis, validation and sensitivity of the data.

Initially it has been described the characteristics of the wave flume and the wave that is reproduced in it, and then the measuring methods as ADV and PIV, in addition to the probes which measure the pressure and the level of the free surface.

Later it was explained how the program UVMAT works for deciphering the data obtained, which allows to obtain the velocity of the particles.

Of great importance is the validation of the data which is carried by the correlation made by UVMAT and by the comparisons between data collected by ADV and PIV.

This was followed by a sensitivity analysis of the data obtained.

3.1 Experiments setup

THE PURPOSE of this thesis is to study what happens in the chosen zone considering the phenomena on a global scale and then later analyse the phenomena that occur on a local scale.

The experiments were performed in a $36m$ long, $0.55m$ wide wave flume (Figure 3.1). The flume is filled with *Polymethyl Methacrylate* (also known as Plexiglas) sediment of low density ($1180kg/m^3$) forming a beach. The median diameter of the sediment is $d50 = 0.64mm$. The corresponding fall velocity is $21mm/s$ [see *Grasso et al., 2009, 2011a*, for more details on the experimental facility]. The wave forcing is produced by a computer controlled piston type wave maker. There is no wave absorption on the wave maker motion.

Figure 3.1. Wave flume in laboratory LEGI

Capacitive wave gages are placed in the cross shore direction of the beach to measure free surface elevations. Beach profiles are recorded between wave series using an acoustic profiler mounted on a motorized trolley. Vertical profiles of the cross-shore velocity are measured at $x = 21.3m$ away from the wave maker with an *Acoustic Doppler Velocity* (ADV)(Figure 3.2).

The wave climate is a repetition of a specific wave sequence of duration $T = 41.75s$ and the wave length is of $2m$. It results from the concatenation of two bichromatic packets with a carrier wave period of $1.7s$ and a packet

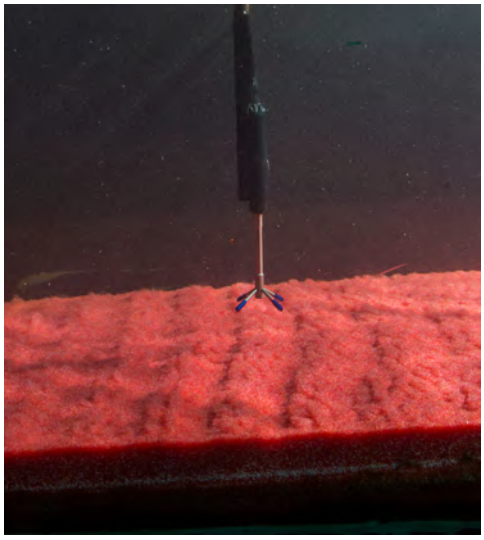

(a) ADV in the wave flume in LEGI

(b) Cloud of particles during an experiment in LEGI

Figure 3.2. Photos of experiment

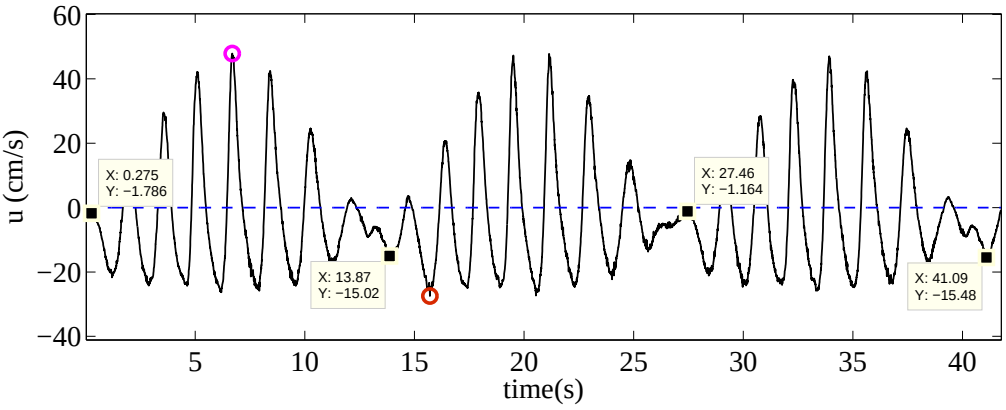

Figure 3.3. Velocity U on time in x=7cm, y=12cm (depth -12,06 cm)

period of 13.6s. The two bichromatic groups can be distinguished: the first between $t = 0.275s$ and $t = 13.87s$, the second between $t = 13.87s$ and $t = 27.47s$, the third between 27.46s and 41.08s which is the repetition of the first one (Figure 3.3). The difference between the two kind of packets is that the first starts with an half circle characterized by crest, indeed the second packet starts with an half circle characterized by through. For the similitude of Froude it was used a length of wave scaled of 1 : 10 i.e. the wave that we consider is 10 time smaller than the wave in nature, so my wave length is 2m so that means in nature this length correspond to 20 m.

The longitudinal section is divided into zones each having a length of 30cm. This study focuses on zone 2, which corresponds to the area between 21m and 21.3m. In the Figure 3.4 it can be seen the representation of the profile of the bottom and an enlargement of the study area where the red rectangle indicates the area of first experiment (0.3x0.24 m) and blue rectangle indicates the area of second experiment (0.05x0.075 m).

In the second part of the research, it was conducted various experiments with purpose to better focus the phenomenon of plug flow. By PIV was recorded with a camera (*Phantom MIRO M310*) what happens into the seabed to the passage of two wave packets with the same characteristics of the previous experiment (Figure 3.5).

It was also used a ruler fixed into seabed with 3 sensors which measure the pressure positioned at x=21,3m, a gauge that measures the height of the free surface and an external removable ruler required for calibration of the images.

Each pressure sensor is positioned at a distance of 1.5cm from the next and the sensor further away from the bottom of the channel is at a distance of 43cm from the bottom of the channel (corresponding to -17cm under free

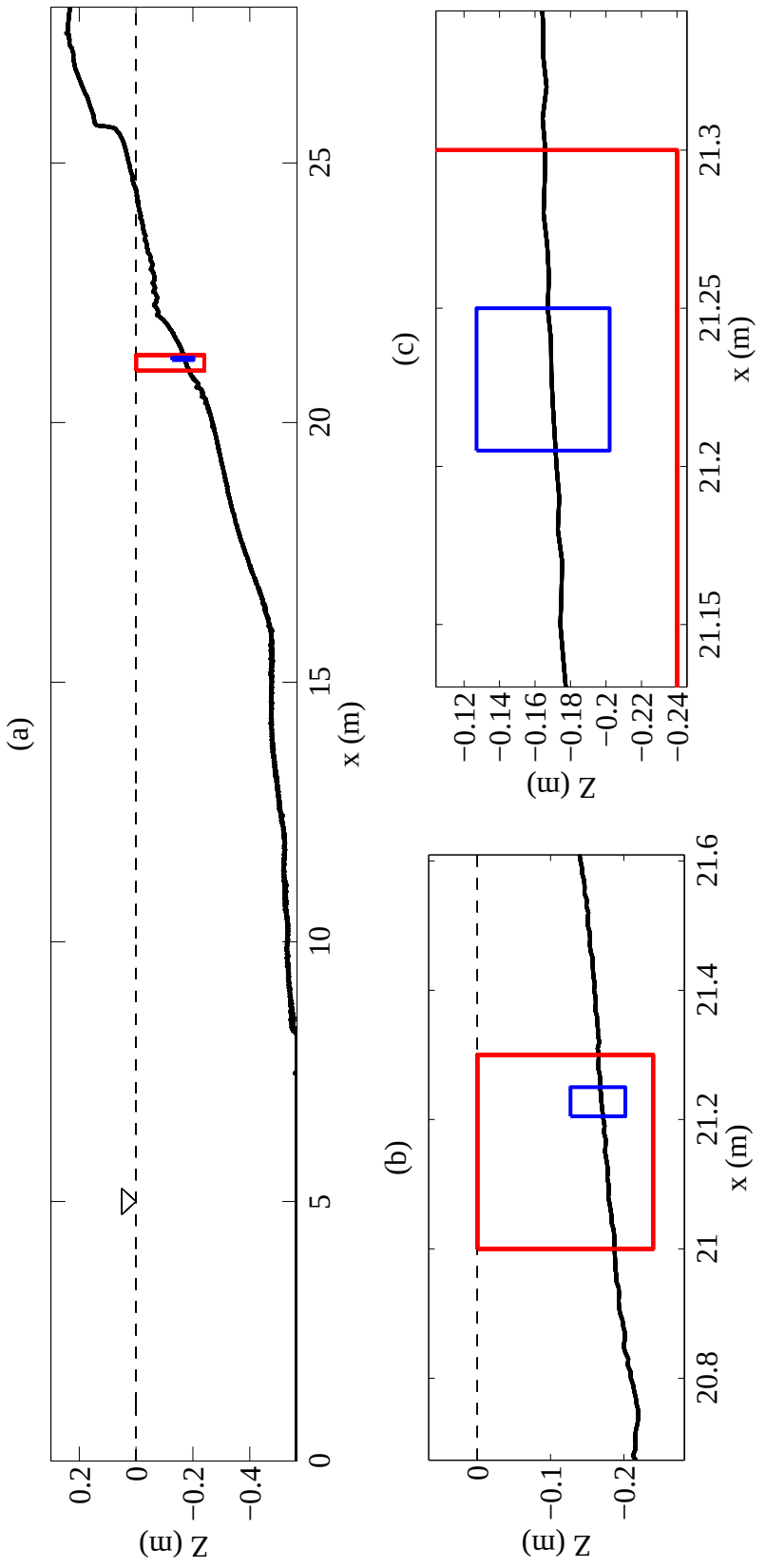

Figure 3.4. Longitudinal profile of the bottom and zoom in the zone of study

Figure 3.5. Camera Phantom MIRO M310

surface level), while the distance of the free surface without waves from the bottom of the channel is of $60cm$ (Figure 3.6).

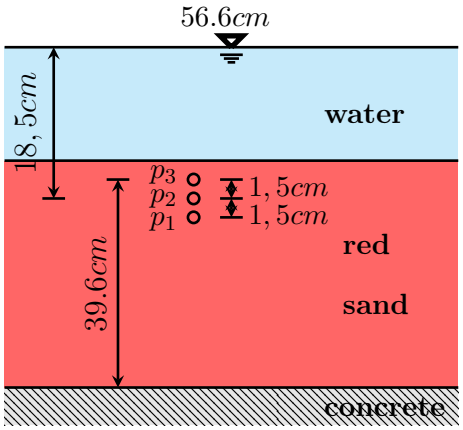

Figure 3.6. Position of pressure sensors

The camera is positioned at the same height of the interface between particles in motion and static particles and each experiment was filmed for $27.7sec$ enough to see the two wave packets. Important is the source of light because it allows to better focus the particles, so were used 2 led lamps positioned as close as possible to the channel.

In each experiment a parameter was changed and the others were remained constant, in order to study the influence of each parameter.

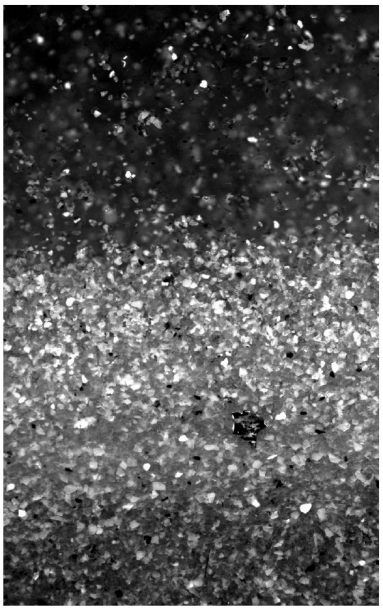

Figure 3.7. Image of second experiment

The parameters considered are:

- frame for second (fps);
- focus for lens of the camera;
- resolution of image;
- exposure of time;
- conditions at the beginning of the movie.

After it is analyzed the experiment 7 characterized by the following values of parameters:

- fps = 300;
- focus lens of camera is 6 times the focus lens used in the previous experiment; resolution = 1280x800 (Figure 3.6);
- exposure time = 500;
- conditions at the beginning of the movie: recording after a few minutes into the experiment.

After calibrating the image, it can be calculate the following information:

- 1 cm = 170 pixels;
- 1 pixel = 0.006cm;
- 1 grain = 11 pixels.

3.2 Measurements: difference between *PIV* and *ADV*

In these experiments, the velocity of the particles was measured in two ways: *PIV* and *ADV*. Now it was described their characteristics.

ADV: The Acoustic Doppler Velocimetry (ADV) is designed to record instantaneous velocity components in a precise volume with a relatively high frequency. Measurements are performed by measuring the velocity of particles in a remote sampling volume based upon the Doppler shift effect (Voulgaris and Trowbridge 1998, McLelland and Nicholas 2000). The probe head includes one transmitter and four receivers.

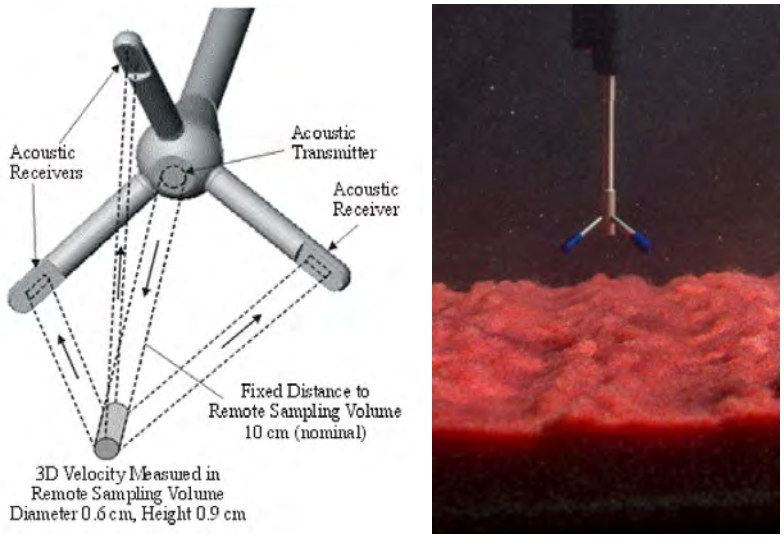

Figure 3.8. Example of ADV with its description and an ADV of LEGI

The remote sampling volumes are located typically between 4 and 7.4cm from the tip of the transmitter. The sampling volume size is determined by the sampling conditions and manual setup. In a standard configuration, the sampling volume is about a cylinder of water with a diameter of $6 - 10mm$ (Figure 3.8). A typical ADV system equipped with N receivers records simultaneously $4 \times N$ values with each sample. That is, for each receiver, a velocity component, a signal strength value, a signal-to-noise and a cor-

relation value. The signal strength, signal to noise and correlation values are used primarily to determine the quality and accuracy of the velocity data, although the signal strength (acoustic backscatter intensity) may related to the instantaneous suspended sediment concentration with proper calibration (Chanson et al. 2008a). Indeed, when the intensity is high, it means that the concentration is very small and when the intensity is little, it means that the concentration is elevated. The velocity component is measured along the line connecting the sampling volume to the receiver each $1mm$. In (Figure 3.9) it can be seen the horizontal velocity and the intensity recorded by ADV. When the intensity is blue means that here there is the bed layer or there is the cloud of particles that appears at the end of wave packet. From the graph of velocity it can be seen two wave packets and a particularity: by the data of intensity you can individuate where is the bed layer, so the fact that the ADV has calculated velocity in the bed layer is a systematic error due to the many reflections of the signal between particles of the bed. Using the program *Vectrino Profiler (Nortek)* is possible to transform all data in Matlab file.

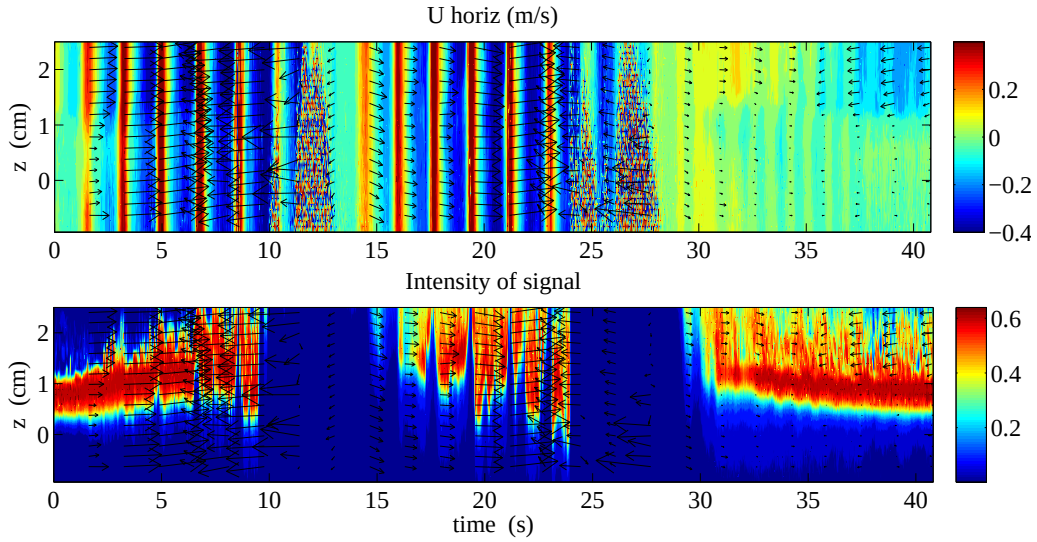

Figure 3.9. Velocity U and normalized intensity measured by ADV

PIV: Other instrument is the particle image velocimetry (PIV), a laser-based imaging technique. Though many forms of PIV exist that extend the technique beyond the original planar two-component velocity measurement capabilities, the basic PIV system consists of a light source (laser), a camera, tracer particles, and analysis algorithms. The imaging and recording parameters, the light source, and the algorithms are adjusted to optimize the recording for the flow of interest and obtain valid velocity data. Common PIV investigations measure two-component velocities in a plane at a few frames per second. However, recent developments in instrumentation have facilitated high-frame rate ($> 1kHz$) measurements capable of resolving transient flows with high temporal resolution. The PIV system used in this research consists of two light sources and one camera (Phantom MIRO M310) (Figure 3.10). PIV determines a velocity field by tracking the aver-

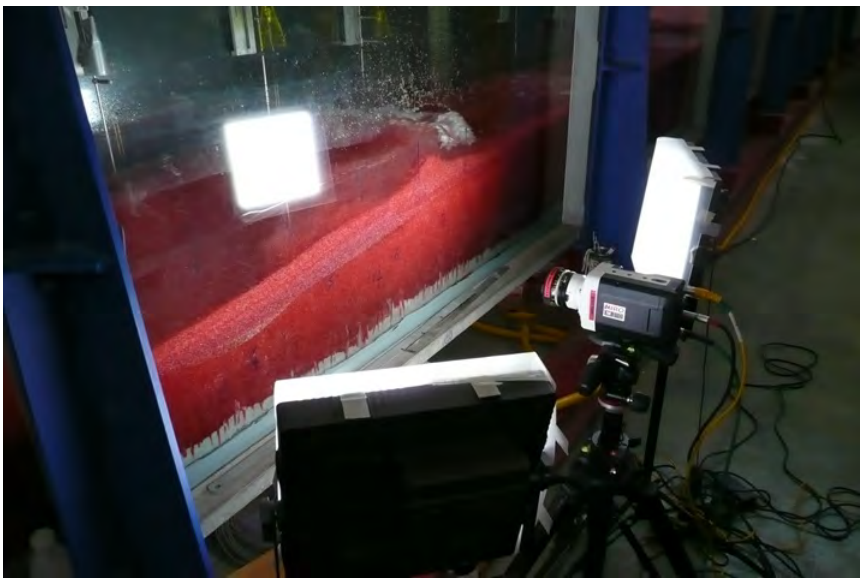

Figure 3.10. PIV system and instruments

age motion of particle groups from a pair of images that are separated by a known time delay. Each image is divided into a grid of regularly spaced interrogation windows. An algorithm computes the cross-correlation function

for all interrogation windows, resulting in one displacement vector per interrogation window and therefore produces a regular grid of vectors. Dividing the displacement vector field by time delay then determines the velocity vector field. The number of pixels on the camera chip then determines the spatial resolution. A seeding density of $8 - 10$ particles per interrogation window is generally desired to aid the cross-correlation function.

3.3 *UVMAT*: how it works

THE PACKAGE UVMAT can be used to visualize, scan and analyse a wide variety of input data: all image and movie formats recognized by *Matlab* and *NetCDF* binary files. It is however particularly designed for laboratory data obtained from imaging systems: the package includes a Particle Image Velocimetry software.

NetCDF (Network Common Data Form) is a machine-independent format for representing scientific data, suitable for large arrays. The NetCDF format has been initially developed for meteorological data, but has been progressively chosen by many scientific communities. This format has been for instance proposed by the European network PIVNet[1] to inter compare data obtained by various techniques of Particle Imaging Velocimetry. Before starting to process the images, it is necessary to perform a geometric calibration of images. The geometric calibration consists in the conversion of the system of units of measurement transforming the pixels in cm. In the first experiment it was used a ruler, so it was get that $1cm$ corresponds to 33.4 pixels and then a pixel measures about $0.3mm$. Because the $d50$ is $0.64mm$, it means that a particle corresponds to about $2 - 3$ pixels. There are 5 modalities to process the images and in these experiments it was used

[1] `http://www.meol.cnrs.fr/LML/EuroPIV2/Proceedings/p251.pdf`

two of them:

- The option civ_series gives access to the PIV processing. The CIV process involves a succession of iterative operations which can be used to improve the results. There are several sequences to obtain results:

  civ1 : the initial image correlation process which by itself already provides a velocity field;

  fix1 : detection of 'false' velocity vectors according to different criteria;

  patch1 : interpolation and filtering on a regular grid, providing access to spatial derivatives of the velocity (divergence, curl, strain);

  civ2 : provides a refined calculation of the velocity field, using the civ1 result as previous estimate;

  fix2 and patch2: similar as fix1 and patch1, but applied to the civ2 results.

- The option merge_proj is used to project a whole series on a given grid or to create a file series by concatenation of different fields. This option allows to merge several field series in a single one. This is useful to merge fields obtained with different cameras. Select the different series, using the input option append. In this case, it is generally useful to interpolate the fields on a single grid. For that purpose it was selected a projection object of type 'plane' with projection mode 'interp_lin' and characterized by a mesh of 0.7mm.

To process images it can select the time interval of images: the program processes two successive images and, before moving on the next two images, jumps the number of images in the range indicated. In this way it can change

the interval of the images, but the time interval (equal to 1 / frequency) is always maintained the same for all analyses.

The time interval of the image pair must be chosen sufficiently small to provide a good image correlation, and sufficiently large to provide good measurement precision. For that purpose the first choice was a range of 5 images, but losing too much data it was chosen then an interval of one image.

Concerning the correlation, it must be set the size of the correlation box and the size of the search box. The correlation box is a set area, composed by pixels having different intensity of color, that the program must recognize identical or very similar in the next image inside the area of search box. The search box instead is a set area in which the program must seek the correlation box. The first step was to estimate Civ1, so it was chosen a correlation square box of side equal to 25 pixels and a search box square with a side equal to 55 pixels, while for the most accurate calculation Civ2 it was changed the correlation square box of side equal to 21 pixels .

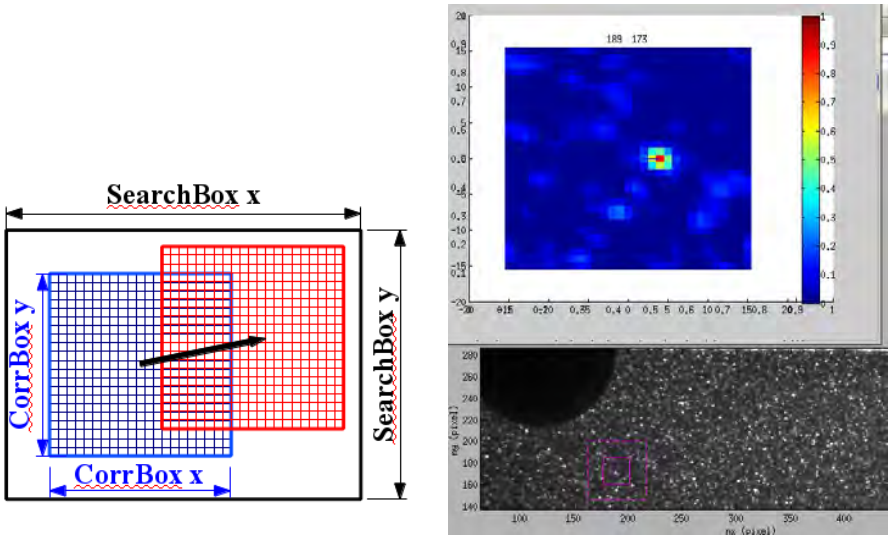

Figure 3.11. Correlation in UVMAT

The Figure 3.11 shows the correlation process and the correlation box and the search box explained before. The two boxes are characterized by a grid that determines the positions of measured velocity vectors: the program sets the vectors in the central positions of the correlation. A default regular grid can be set by the meshes Dx=10 and Dy=10 (in pixels), alternatively a custom grid can be stored in a text file and selected by the check box get grid. Sometimes it is convenient to limit the processing to a sub region, selected by a mask image, to optimize the resolution (Figure 3.12).

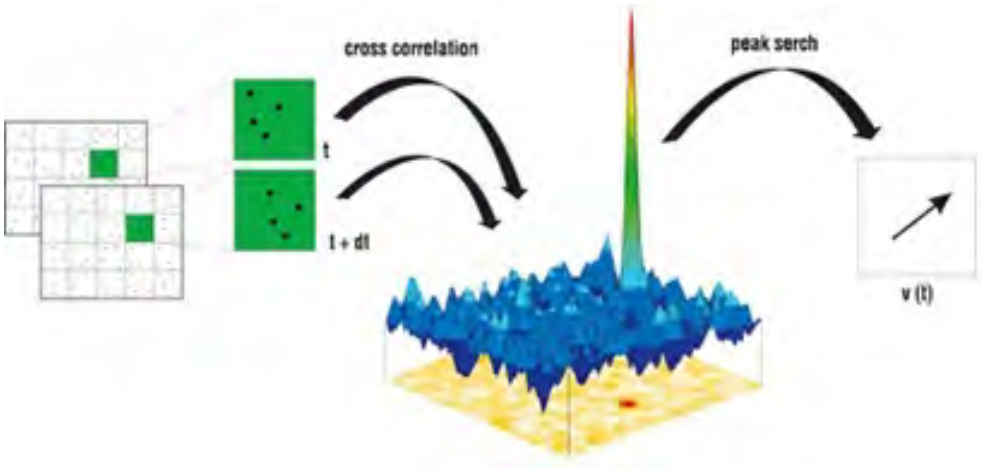

Figure 3.12. UVMAT processing to obtain the velocity field

In the experiments it was used a camera Phantom Miro 1280x800 pixels and it was processed the images with *UVMAT*: it has got an excellent spatial resolution depending on the choice of the mesh, as it will see below in Figure 3.14.

Concerning the temporal resolution various tests were carried out. Considering that the movement of the correlation box within the search box is 1/4 of the size of the correlation box, the best temporal resolution for the global experiment is 160 images for second and means that DT is equal to 0.00625s, while in the local experiment is 300 images for second i.e. DT is equal to 0.00333s

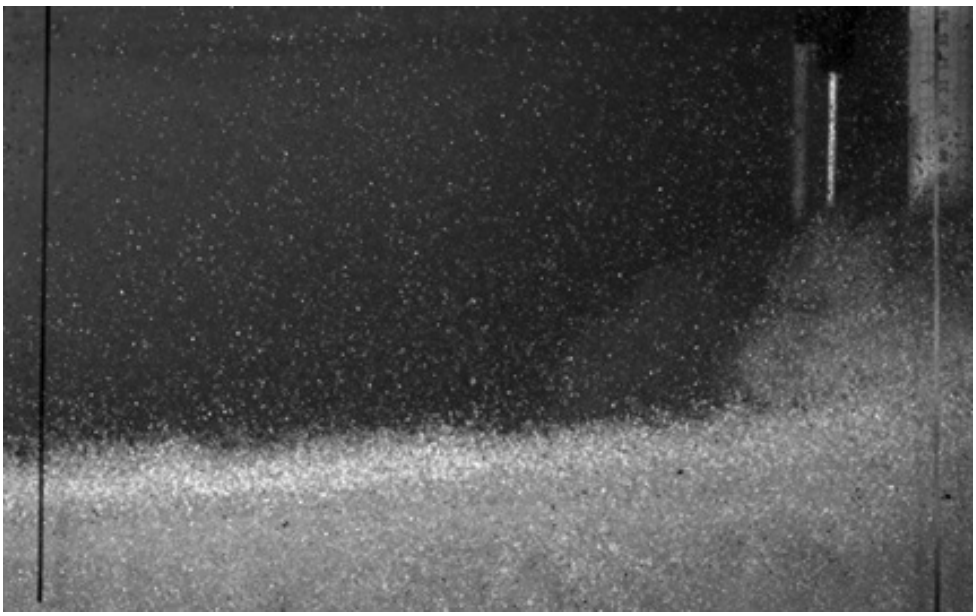

Figure 3.13. Example of input for UVMAT

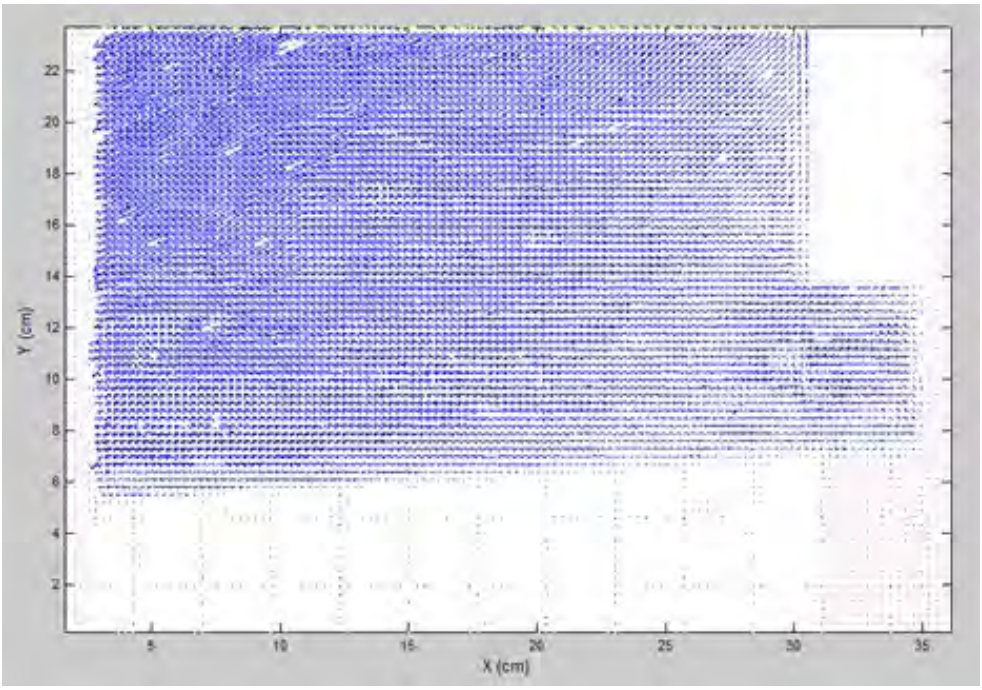

Figure 3.14. Example of output for UVMAT

3.4 Validation of data

BEFORE ANALYZING the data obtained from instruments or programs of calculation, it is good practice check the accuracy of such data. To validate the data that will be used in the analysis of the first experiment, it was made the comparison of horizontal velocity measured by the two instruments used, PIV and ADV. Instead to validate the data concerning the second experiment, it was attempted to maximize the correlation in the process of calculating the velocity in UVMAT.

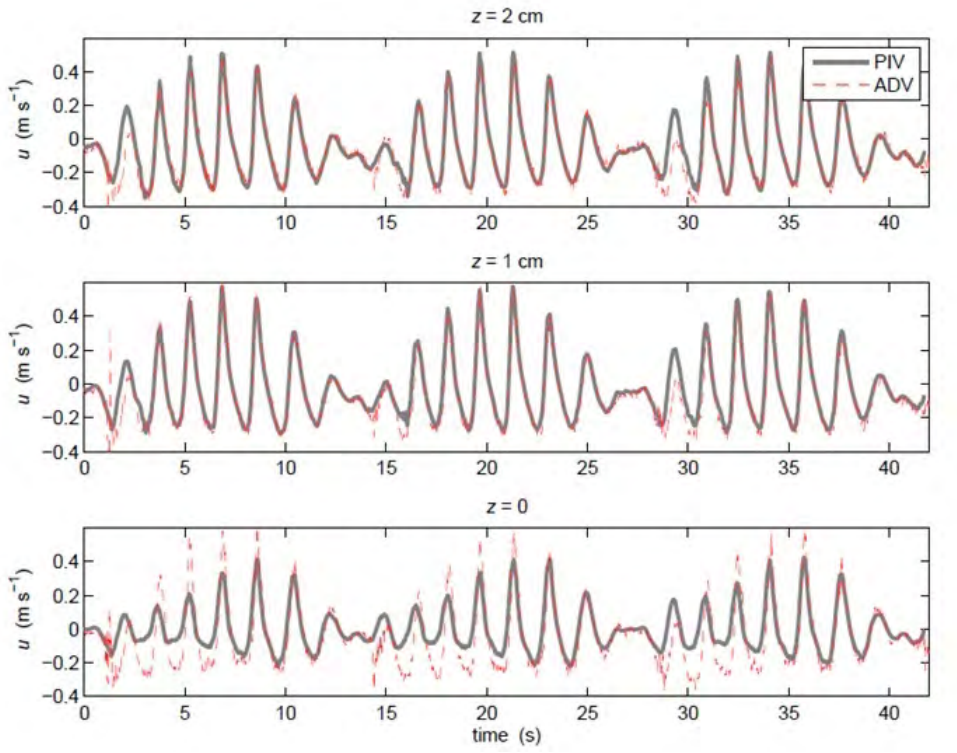

Figure 3.15. Comparison of velocity U between ADV and PIV

It can be seen in the Figure 3.15 the comparison of the horizontal velocity obtained by the two different instruments. Each graph is referred to a different distance from the bottom which correspond to z=0: the first one represents the horizontal velocity measured in z=2cm, the second one in z=1cm and the third one in correspondence to the bottom. Until ADV is

positioned away from the bottom it provides the same values provided by PIV, and this is a validation of the value of velocity calculated by *UVmat*. Instead when the ADV is positioned closer to the bottom the two measurements are completely different and this means that to examine the layers of the bottom it must be used the PIV method, because the ADV is disturbed by grains, while PIV is external to flume and so it isn't disturbed. It may be noted that in z = 2cm the maximum value of the velocity is lower than the maximum value of the velocity measured in z = 1cm. This is due to the phenomenon of 'overshoot' which is visible if it is observed the profile of horizontal velocity along the vertical, but this will be explained in the following sections.

Regarding the validation of data of second experiment analyzed, it was done a lot of tests to choose the best values of calibration parameters for analysis with *UVMAT* and create the files '.nc'. It was chosen a pair of images each 500 images around and for each pair it was changed the value of parameters for calibration of correlation. Here it was shown only 3 cases considering:

- A pair in a crest: images=2888-2889;
- A pair in a reversal flow: images=2956-2957;
- A pair in a through: images=3168-3169.

The Table 3.1 shows the 4 different combinations of values of parameters (in pixel) and the combination that it was used in the processing.

Once the program UVMAT has calculated velocity vectors, it represents them in arrows of length equal to the vector module and it colors them of red, green or blue respectively if its correlation is bad, acceptable or good. For each combination it was improved the values of correlation, decreased

Table 3.1. Combinations of values of parameters for the correlation (pixel)

	Corr choosen	**Corr 1**	**Corr 2**	**Corr 3**	**Corr 4**
CorrBox1	100	25	50	75	90
SearchBox1	180	50	110	165	200
Grid 1	40	40	40	40	40
CorrBox2	85	21	42	63	85
Grid 2	20	20	20	20	20

the number of red and green arrows, so it was used 2 ways to validate the choice: in the first way it was visually improved the number of blue arrows and in the second way it was calculated the RMS of all value of correlation and it was tried to improve this number. So the Table 3.2 shows that the chosen combination of values of parameters is better than other combinations.

Table 3.2. Correlation for each combination

	Crest	**Reversal flow**	**Through**
Corr choosen	0.9134	0.9487	0.9044
Corr 1	0.8283	0.8282	0.8248
Corr 2	0.9005	0.9062	0.8954
Corr 3	0.9117	0.9323	0.9043
Corr 4	0.9130	0.9503	0.9041

After the choice of the best values of parameters for the correlation, it was used the command 'mprog' and so it was chosen a grid mesh of $0.07cm$, which is approximately the size of one grain.

3.5 Sensitivity

BEFORE TO ANALYZING the data, it was made some design decisions about how to study the information obtained:

- temporal resolution: DT;
- spatial resolution: DX and DY;
- section of study: coordinate x.

First of all it was analyzed the choice of the interval DT of the images: obviously using all data obtained the results are complete, but when these are numerically excessive appears in the results the 'noise'. So the preliminary analysis is aimed to finding if it is possible to reduce the number of images to analyse. The available information are of 6680 images for the first experiment and of 8310 images for the second experiment, so only access to a supercomputer it can allow an analysis of full information.

It was desirable to reduce the images by a factor DT and this case has been tested. For this it was tried to analyse the data considering an interval of 5 images, i.e., *UVMAT* analyses two successive images and then it jumps 5 ones to analyse the following two images.

In terms of processing time, this choice increases the speed of analysis of 5 times but, as it can be seen from Figure 3.16-3.19, the risk to lose data may be important. Figure 3.16-3.19 show the horizontal velocity in the same test in Zone2 in 2 different depth: the first pair of graph is regarding the Zone2 in z=1cm from bottom(the second graph is an enlargement of a peak event) and the second pair is regarding the Zone2 in z=2cm from bottom (the second graph is an enlargement of a peak event). It can be seen in these figures as the choice of interval affect the determination of the results, especially in the Figure 3.19.

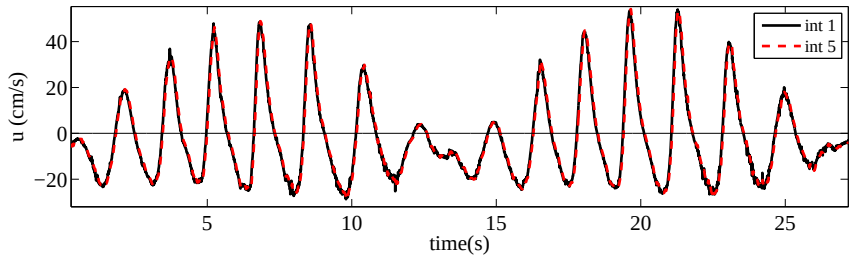

Figure 3.16. Velocity U on time in Zone2 in z=1cm from bottom (y=8.33cm, x=25cm)

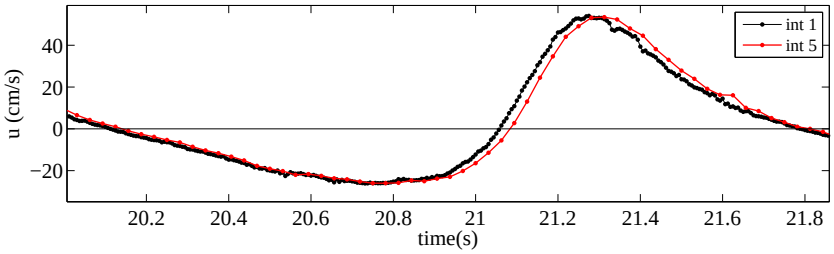

Figure 3.17. Zoom of velocity U on time in Zone2 in z=1cm from bottom (y=8.33cm, x=25cm)

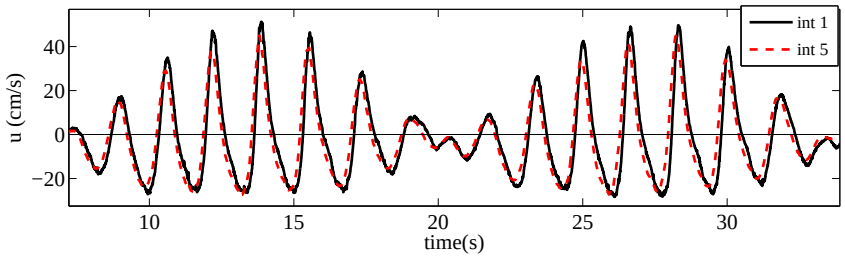

Figure 3.18. Velocity U on time in Zone2 in z=2cm from bottom (y=9.31cm, x=25cm)

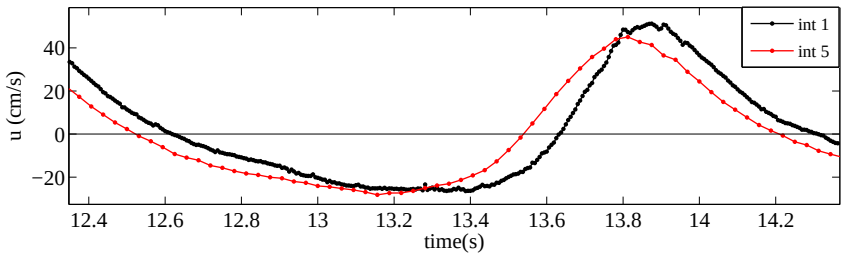

Figure 3.19. Zoom of velocity U on time in Zone2 in z=2cm from bottom (y=9.31cm, x=25cm)

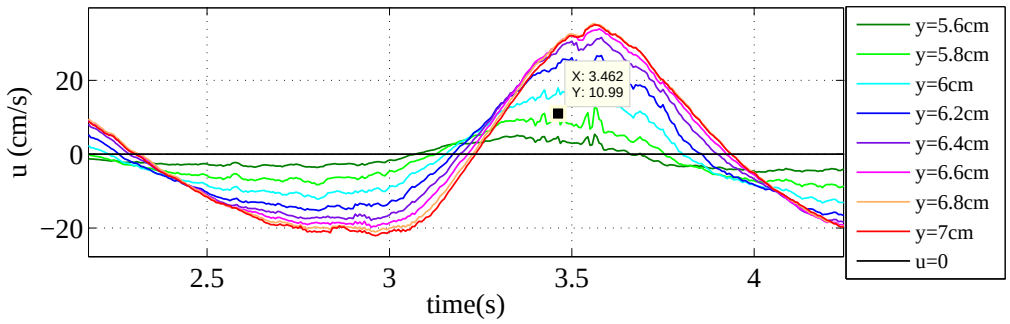

Figure 3.20. Velocity U on time in Zone2 with mesh 2mm (x=7cm)

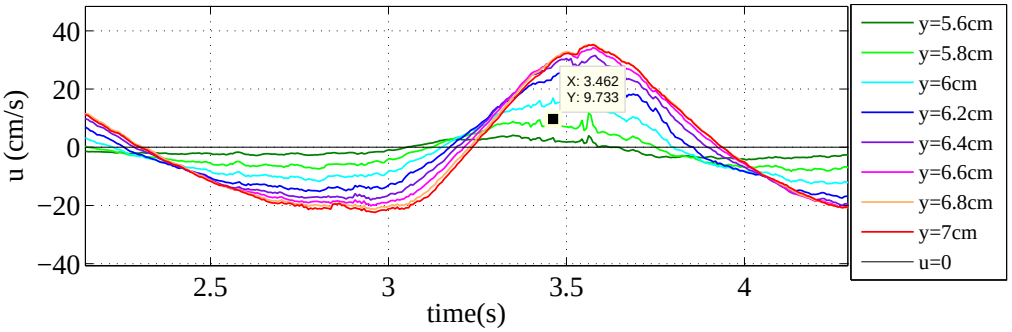

Figure 3.21. Velocity U on time in Zone2 with mesh 0.7mm (x=7cm)

Concerning the choice of the spatial resolution, the processing time could be reduced implementing the mesh of each image. So it was chosen to first test a square grid where DX = DY are equal to $2mm$ and it was compared with a square grid with DX = DY equal to $0.7mm$, around the size of one grain. It can be noted that the spatial resolution is so important that to describe the subject of study it is necessary considerer all data, even if greatly increases the processing time, so it was chosen a grid with DX = DY equal to $0.7mm$. Looking at the Figure 3.20 and Figure 3.21 it can be seen the influence of the choice of the grid by comparing the values of the horizontal velocity at the point highlighted with the same coordinate x. Indeed in the first graph the velocity is calculated with a grid of 2mm and the value is 10,99 cm/s, while in the second graph the velocity is calculated with a grid of 0.7mm and the value is 9,733 cm/s that is smaller than the

other.

Finally it was chosen a horizontal spatial coordinate on which to report all measurements. Because the choice is conditioned by the boundary conditions of the experiment, it was chosen the coordinate $x = 7cm$, because it is a coordinate sufficiently far away from the left edge of the image and far enough away from the instrument ADV positioned to the right of the image and from the particle cloud that is created during the experiment.

Chapter 4

Results and discussion

THIS CHAPTER is composed of two sub-chapters which deal respectively with the analysis of the results of the first experiment, called global, and the second experiment, called local because it is the zoom of a part of the study area of the first experiment.

4.1 Global analysis: 1^{st} Experiment

It was initially studied the velocity profile over time and along the vertical and were calculated some quantities statistics like the mean, standard deviation and skewness.

Of great importance is the determination of the interface which separates the particles moving from static ones, since then allows to identify the formation of plug flow and the depth of erosion that it produces.

Then it compared the time series of velocity in different bottom depth with the results obtained from Zala-Flores.

It has been studied the dynamics of the formation of plug flow by calculating the acceleration and therefore the number of Sleath S, which constitutes a limit which identifies the formation of plug flow.

Finally were considered three plug flow and have been identified their characteristics.

4.1.1 Profile of horizontal velocity U along the vertical

THIS SUBSECTION analyses the horizontal velocity profile at some given instants. The relevant instants correspond to up and down zero crossing, the maximum and the minimum points of 2 times the wave period. The aim of this is to verify that the profile shape of the horizontal velocity U along the vertical in some points chosen is similar to the profiles shapes velocity along the vertical found by Nielsen. It was represented the horizontal velocity U on time and it was identified the value of the maximum velocity. After choosing a time interval equal to the sum and subtraction of a period with respect to the maximum crest, it was identified the points of zero up crossing, the zero down crossing and minimum points, as in the Figure 4.1.

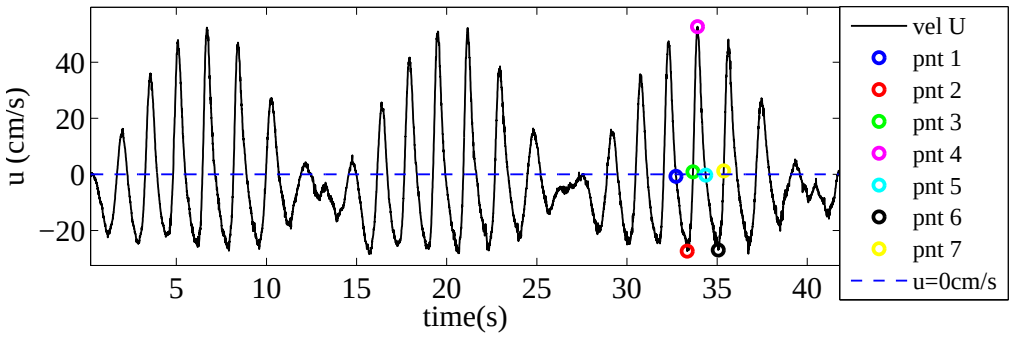

Figure 4.1. Velocity U on time and chosen points (y=18cm, x=7cm, depth -6 cm)

Figure 4.2 shows in the first graph the zoom of the time interval chosen and in the second graph it was represented the velocity profiles along the vertical relative to each instant. In the first $5cm$ along the vertical it can be noted that the velocity is zero for all profiles and this indicates where is the bottom. As soon as it rises above the bottom, it is seen that the velocity increases very rapidly both in the positive direction than in the negative direction in dependence of the point considered. Having considered almost

two periods, it can be seen how the profiles corresponding to the same phase are very similar. The shape of the profiles as expected follows the rules outlined by Nielsen, especially with respect to the profile of the crest where it can be seen clearly the phenomenon of 'overshoot'. The maximum velocity is considered in the depth of $18cm$, corresponding to 6cm under the free surface, and in fact, already from the depth $9cm$, corresponding to 2cm above the bottom, it can be seen a velocity which remains constant along the vertical.

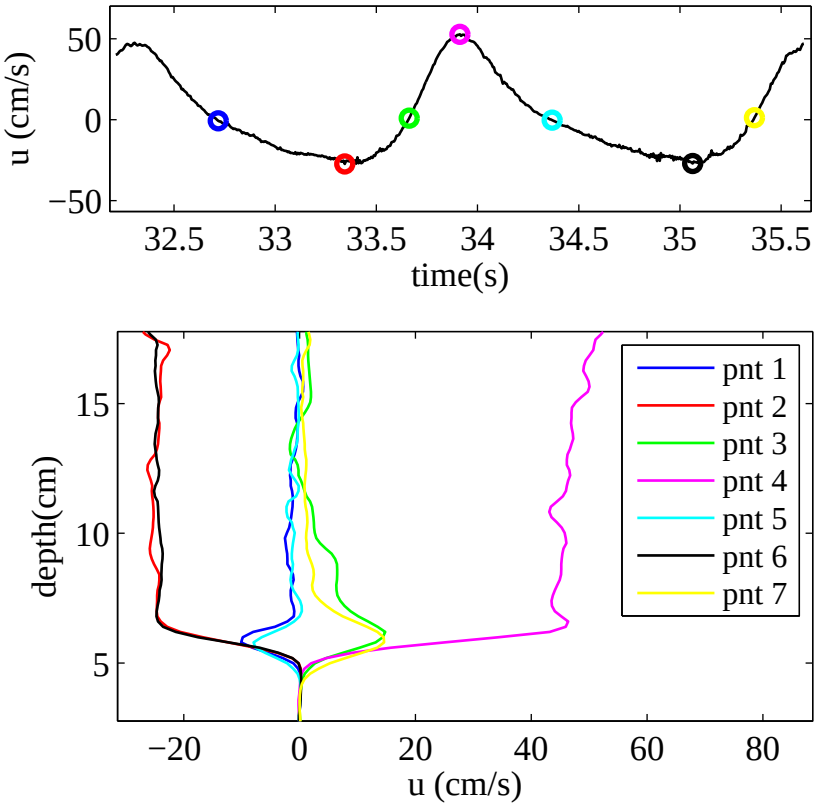

Figure 4.2. Period of max crest with chosen points (y=18cm, x=7cm, depth -6cm) and velocity U on vertical (x=7cm)

4.1.2 Analysis of the behavior of the wave

THIS SUBSECTION aimed to analyzing the behavior of the wave. Figure 4.3 shows the horizontal velocity in relevant depth:

- in y=18cm corresponding to 6cm from free surface and 11cm from the bottom;
- in y=6cm corresponding to 18cm from free surface and is on the bottom;
- in y=5,5cm corresponding to 18,5cm from free surface and 0,5cm under the bottom.

In the spatial coordinate of $x = 7cm$, the interface of the bed is around $6cm$, and it can be observed as approaching the bed the profiles of velocity begin to decline more rapidly. Indeed as moving into the bed in a few mm there is a notable decrease in velocity as suggested by Nielsen referring to the profiles along the vertical seen previously.

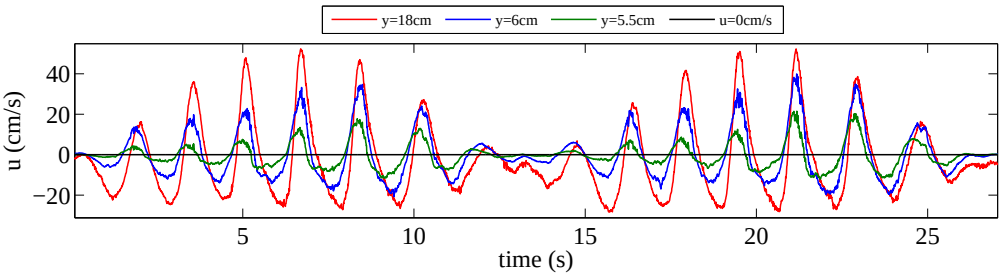

Figure 4.3. Time series of velocity U in significant horizontal sections

Examining the Figure 4.3 it can be noticed the particular shape of the waves with pinched crests and stretched troughs. In particular, it highlights the fact that the value of velocity in the crests is about 50% greater than the value of velocity troughs, and this is evident if it looks at the profile of the velocity of the free surface (red line: $y = 18cm$). This means that

the velocity is skewed. Skewness is a measure of the asymmetry of the data around the sample mean.

$$S_k = \frac{\frac{1}{N}\sum\left(x_i - \bar{x}\right)^3}{\left(\frac{1}{N-1}\sum\left(x_i - \bar{x}\right)^2\right)^{3/2}} \tag{4.1}$$

If skewness is negative, the data are spread out more to the left of the mean than to the right. If skewness is positive, the data are spread out more to the right. The skewness of the normal distribution (or any perfectly symmetric distribution) is zero. Because of the skewness depends by average and standard deviation, subsequently it was reported in the Figure 4.4 the mean, standard deviation and skewness relating the horizontal velocity U in the fixed spatial coordinate. In these plots it is seen the comparison between three cases:

- considering all data (line blue);
- considering three periods around the biggest crest (line magenta);
- considering one period around the biggest crest (line green).

By examining the plots, it can notice:

- The root mean square value of the velocity decreases down to the bed in all cases;
- The mean velocity is negative in the upper part of the profile in the first case, indicating the presence of an undertow, and it decreases deeper down in the boundary layer; In the other two cases the mean velocity is positive and around zero.

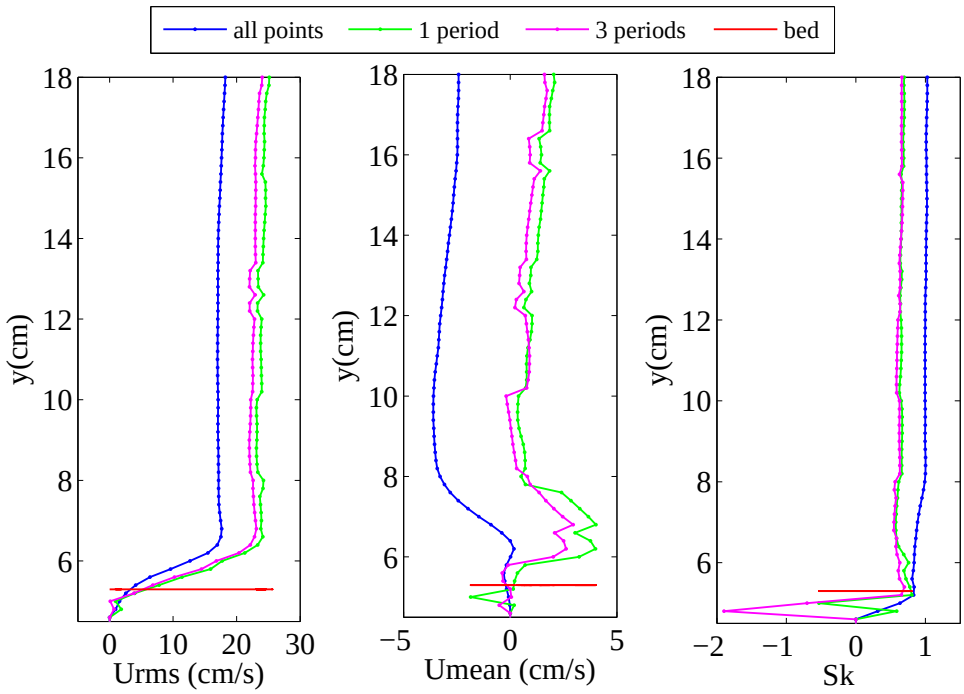

Figure 4.4. Deviation standard, mean and skewness of velocity U considering different number of points

- In all cases the profiles show similar behavior and as was expected the free-stream values of the standard deviation and mean velocity are different;

- In the plot of skewness of velocity it can be seen that the skewness is constant and equal to 1 and it decrease down the bed, because of in this experiment there are more wave symmetric than asymmetric and the average is decreasing down the bed.

4.1.3 Interface between still and moving particles inside the bed

TO STUDY the dynamics of the layers of the bed, it is necessary to identify the interface between the layer of particles in motion and the layer of particles that remain still. It could be chosen a threshold velocity under which particles remain still. Three thresholds were considered:

- 1.1 cm/s;
- 1.0 cm/s;
- 0.8 cm/s.

Figure 4.5 shows the identified bed level relatively to the different thresholds. The difference due to the threshold chosen is minimal and then for subsequent studies it was decided to choose the threshold equal to $1.0 cm/s$ (blue interface). In the calculation of the interface the choice of the grid is very important: if it had chosen a grid of $2mm$, it would have lost many decisive points for the research (Figure 4.6 and Figure 4.7). So it was decided to used the grid as small as possible of 0.7mm.

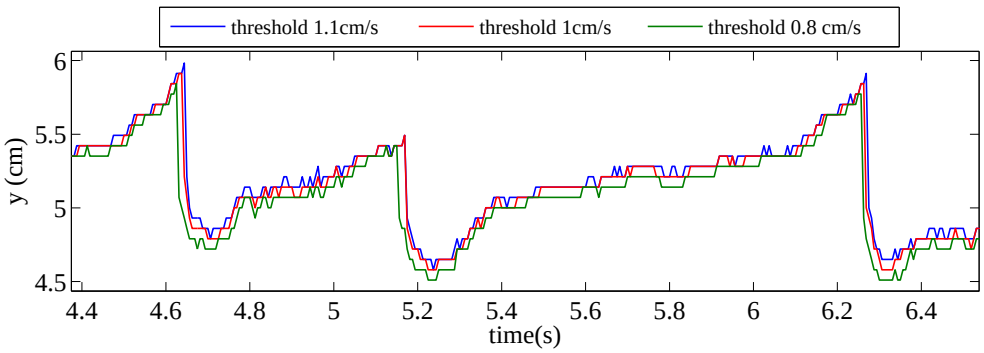

Figure 4.5. Zoom of interface with different thresholds of velocity U: 1.1 cm/s, 1cm/s and 0.8cm/s (x=7cm)

From Figure 4.6 and Figure 4.7 it can be observed a certain asymmetrical behavior. The accumulation process is gradual whereas the erosion is sudden

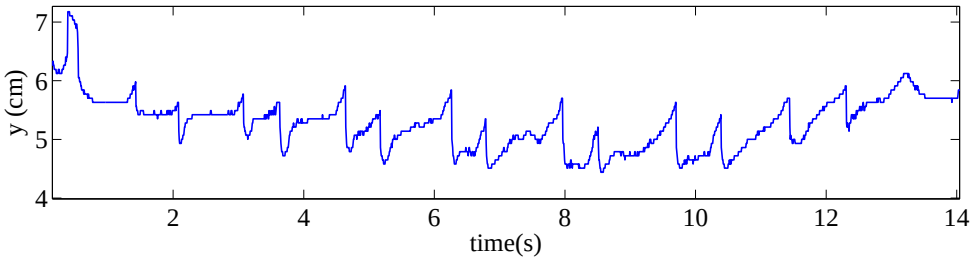

Figure 4.6. Interface with mesh 0.7mm in a packet waves (x=7cm)

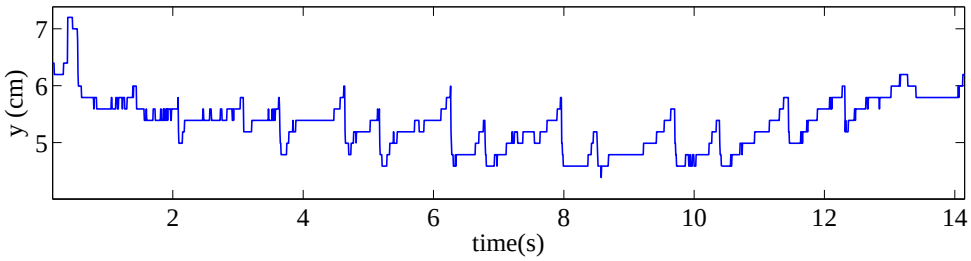

Figure 4.7. Interface with mesh 2mm in a packet waves (x=7cm)

and followed by a stationary condition of a few DT. It can be anticipated that during this little period occurs the phenomenon of plug flow: for some instants, when the flow reverses, sediments start to move as a solid block in the opposite direction respect the flow direction. From the interfaces it can extract two categories of data: the difference in depth in two successive instants, when the flow reverses, indicates the thickness of the plug flow and hence the number of layers that move at the same time; the difference between the start instant and the final instant of the time interval in which there is constant depth, when the flow reverses, indicates the duration of time in which the upper layers at this depth move together.

Now it is possible to identify the points where there are the plugs flow and then where they cause observable erosions. For example, in Figure 4.5 it can be considered the plug flow at $t = 4.6s$ around, it can deduce that the thickness of the layers that move is equal to approximately $1cm$, and since $d50$ is equal to $0.64mm$ it means that 15 layers of particles are moving.

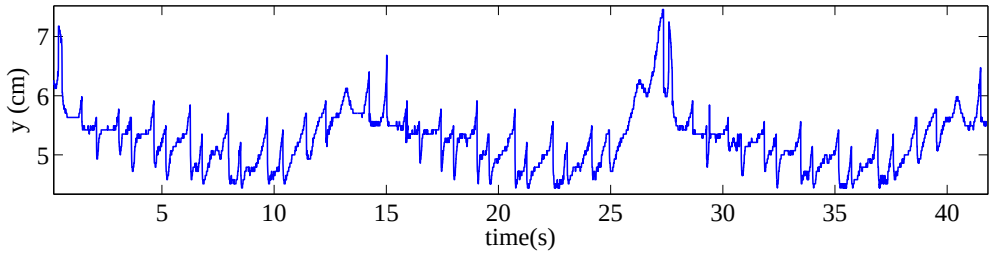

Figure 4.8. Interface with mesh 0.7mm in all time points (x=7cm)

4.1.4 Time series of horizontal velocity U in different depths: comparison with Zala_Flores (1998)

ANOTHER WAY to see the phenomenon of plug flow is analyse the behavior of the layers of bed when the flow is reversed. The definition of plug flow is layers of sediments that start to move as a solid block when the flow reverses. So it is expected that in the moments in which there is reverse flow velocities in the layers in the bed are the same and therefore the profiles of the time series of the horizontal velocity overlap in these instants.

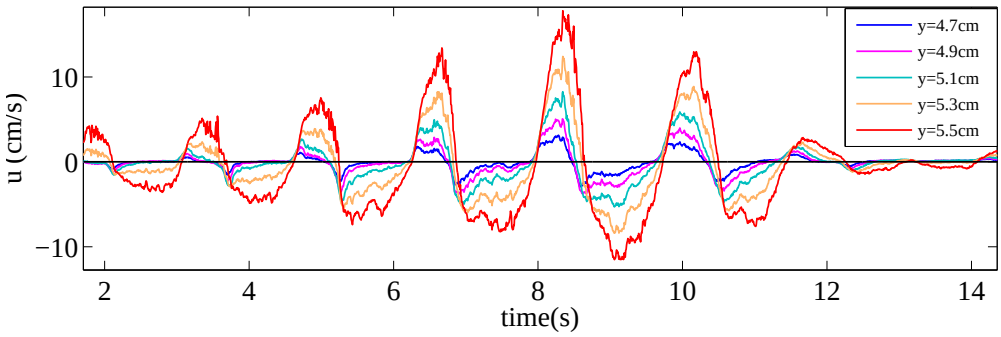

Figure 4.9. Time series of velocity U in the bed in a packet of waves (x=7cm)

Figure 4.9 and Figure 4.10.a show how the velocity varies with time at different depths below the level of the bed (in this section the bottom is at depth y=6cm).

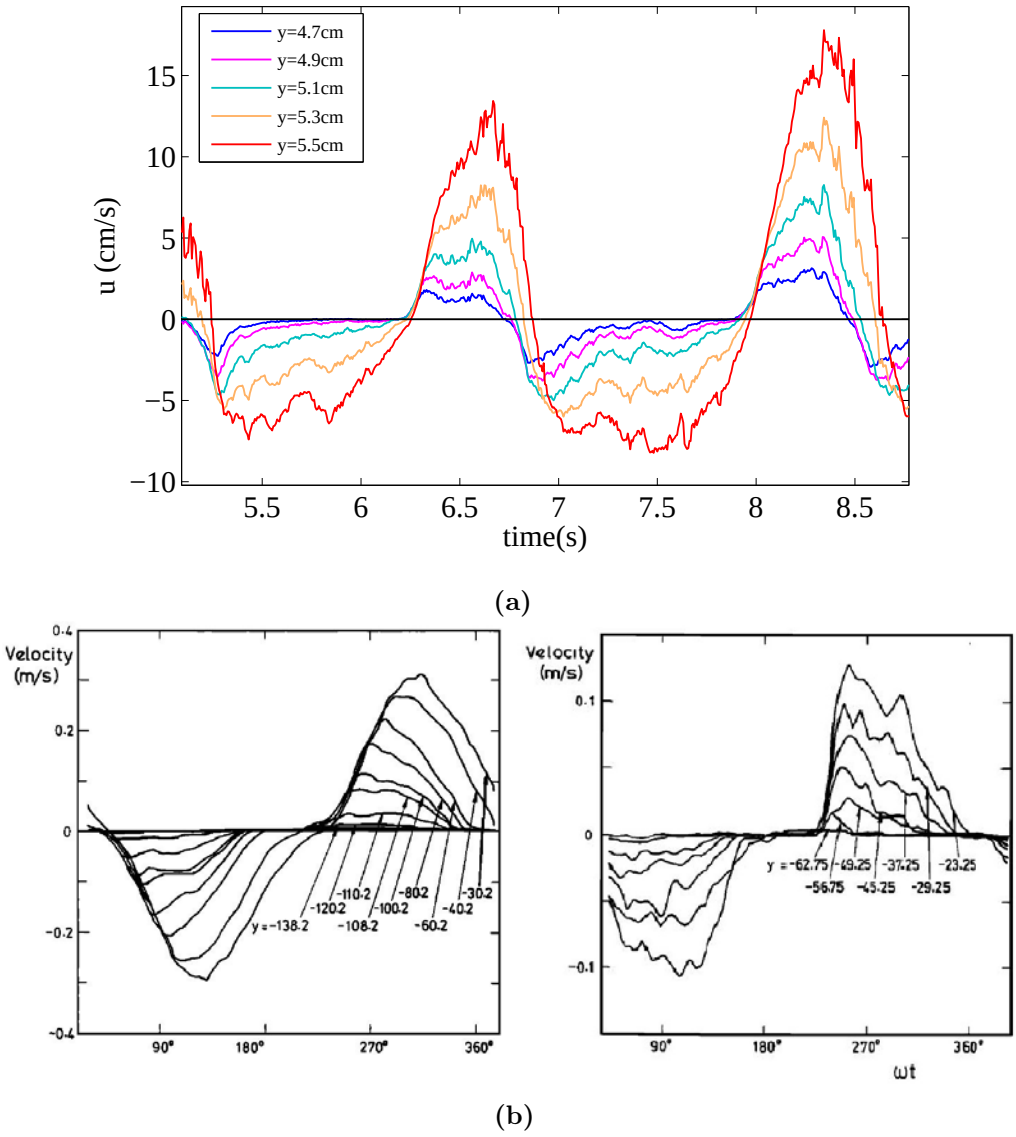

(a)

(b)

Figure 4.10. (a)Zoom of time series of velocity U in the bed in a packet of waves (x=7cm); (b)Time series of velocity U in bed in the Experiment of Zala Flores:on the left case of high value of S number and on the right case of intermediate value of S number

These data are useful for calculating the thickness of the movable layer which determines the plug flow. Indeed considering the instant at which the profiles overlap is sufficient to identify the profiles relating to the maximum and minimum depth in order to obtain the thickness of the plug flow. In the next section will be discussed this subject more extensively.

To be able to make a comparison with the results suggested by Zala-Flores, first of all it was calculated the S number as the standard deviation of all the instantaneous values of S. In this case of study it was calculated a S_{RMS} equal to 0.62 and then according to Zala-Flores, it falls in the case of S value between intermediate and high values. Figure 4.10.b show the two different cases considered by Zala-Flores: in the first case, it was considered the profiles obtained for intermediate values of S and in the second case it was considered the profiles for high values of S. Examining the Figure it can be noticed such as the wave shape in this experiment is similar to that shown by Zala-Flores in the case of intermediate value: crest and thought very jagged and pointed. While comparing the profiles for high values of S number, it can be noticed the similarity regarding to the accentuated displacement of the minimum towards the left decreasing in depth.

4.1.5 Dynamics for plug flow formation and Sleath model [Sleath (1999)]

THIS SUBSECTION aimed to explain the dynamics for plug flow formation that are ruled by the dimensionless number S. As explained in the theoretical part, S number is calculated from the relationship between the acceleration, considered very far from the bed, and a constant depending by the acceleration of gravity and relative density. In this first experiment the limits of the number S were calculated by an approximation. Taking

Equation 2.10 have been neglected:

- the first term in the first member because the thickness of the plug flow normally takes about 20 $d50$, and then makes the term small as to be negligible compared with the order of the other terms of the equation;
- the second term of the second member because it is about the order of 10^{-4}, and then also it is negligible compared with the orders of the other terms of the equation.

For these reasons the limits of the number S are equal to $+/-K_f C^*$ which according to literature is taken approximately equal to 0.35 considering K_f about 0.7 and $C^* = 0.5$. Considering as upper and lower limits $S = 0.35$, it was calculated the limits of acceleration corresponding to those S value of $+/-62 cm/s^2$. When the value of S exceeds these limits the phenomenon of the plug flow occurs: when the acceleration is negative there is decreasing velocity and when the acceleration is positive there is growing velocity.

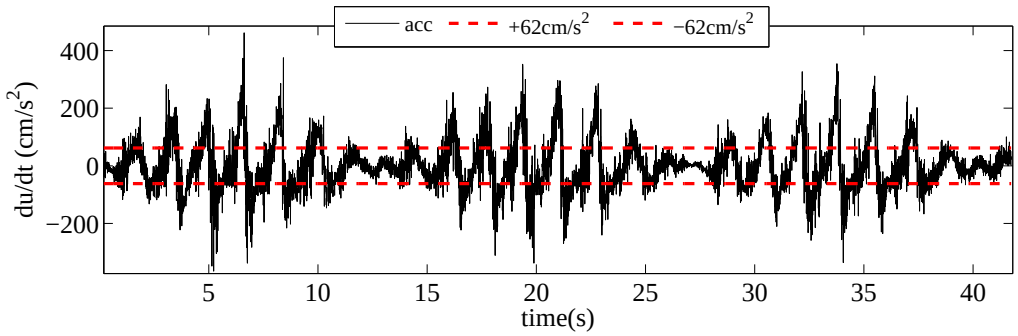

Figure 4.11. Acceleration and limits of acceleration value for plug flow formation(x=7cm, y=12cm, depth -12cm, z=6cm from bed)

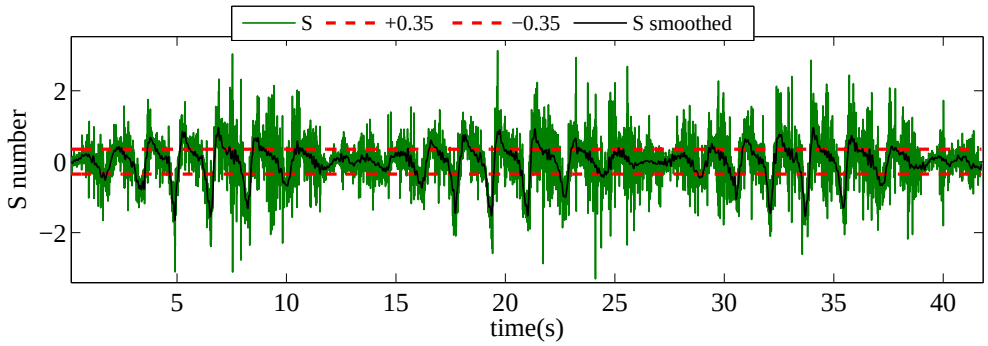

Figure 4.12. Sleath number and limits of S value for plug flow formation (x=7cm, y=12cm, depth -12cm, z=6cm from bed)

The Figure 4.11 and Figure 4.12 show respectively the acceleration and the S number both with the limits represented by two red dotted lines and it can be seen that at the overcoming of such lines will have a plug flow. The acceleration was calculated at the depth y = 12cm because, as seen from the profile along the vertical of the horizontal velocity, already by the depth y = 8cm velocity can be considered constant and equal to the one of the free surface.

To show this concept it was chosen, as example, three points of the interface where it is clear that there is the beginning of the plugs flow (blue, red, green circles) in Figure 4.13. It should be noted in the Figure 4.13 what happens in correspondence of these three moments:

- in the graph of S number it can be seen the exceedance of limits in correspondence of these points;
- in the graph of the horizontal velocity it can be seen each point is in correspondence of through, precisely after little DT where the value of the tangent of the velocity is very high;
- in the graph of the time series of the horizontal velocity at different depths there is the overlapping of the lines in correspondence of these

instants, indicating that all the layers of the bed with that velocity move together and so there is formation of plugs flow.

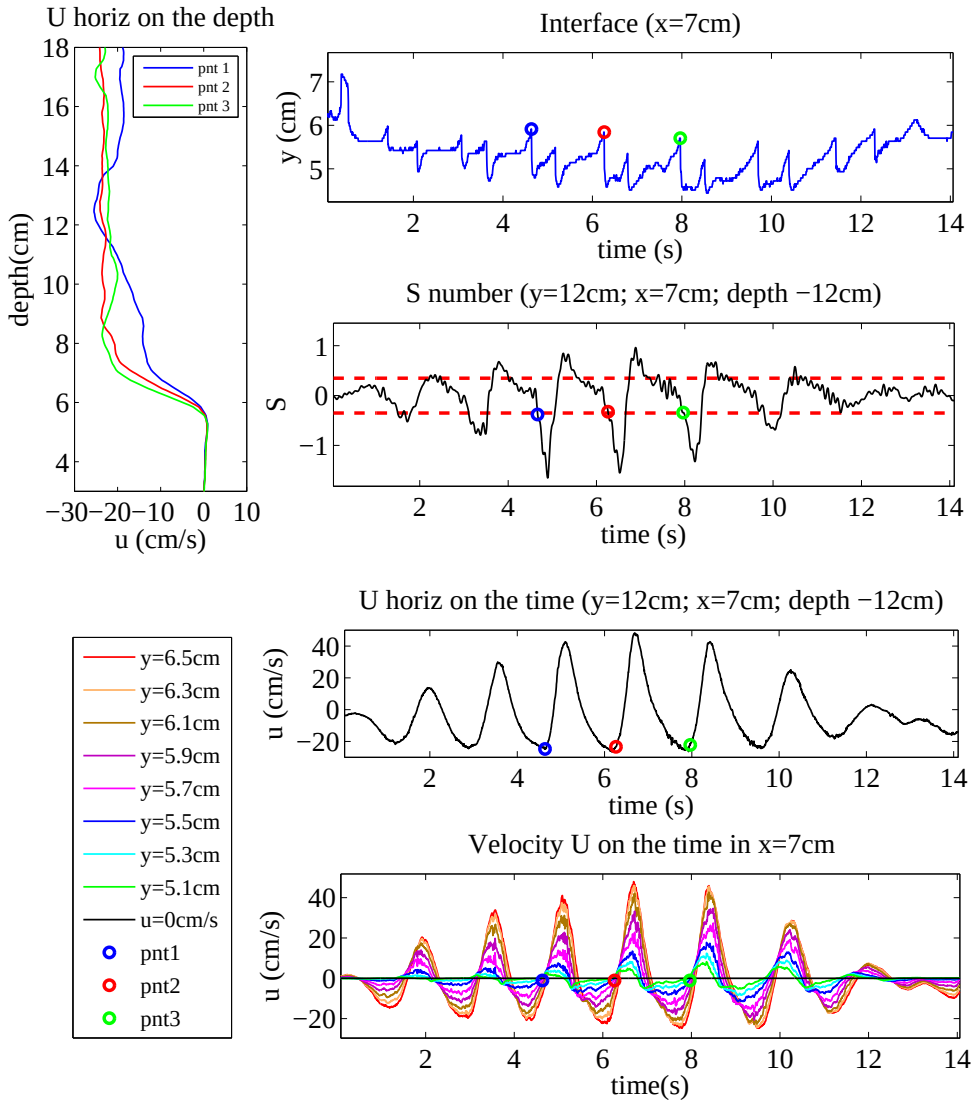

Figure 4.13. Analysis plug flow in t=[4,638; 6,263; 7,963] s

It is interesting now better analyse the data obtained. In each period are always formed two plug flow: one in the rising phase of the wave immediately after the passage of the through and the other is formed in the decreasing phase immediately after the passage of the crest. In this case it was considered around a period of the first wave packet in order to have 3 plugs flow, so the third one can confirm the results of the first one.

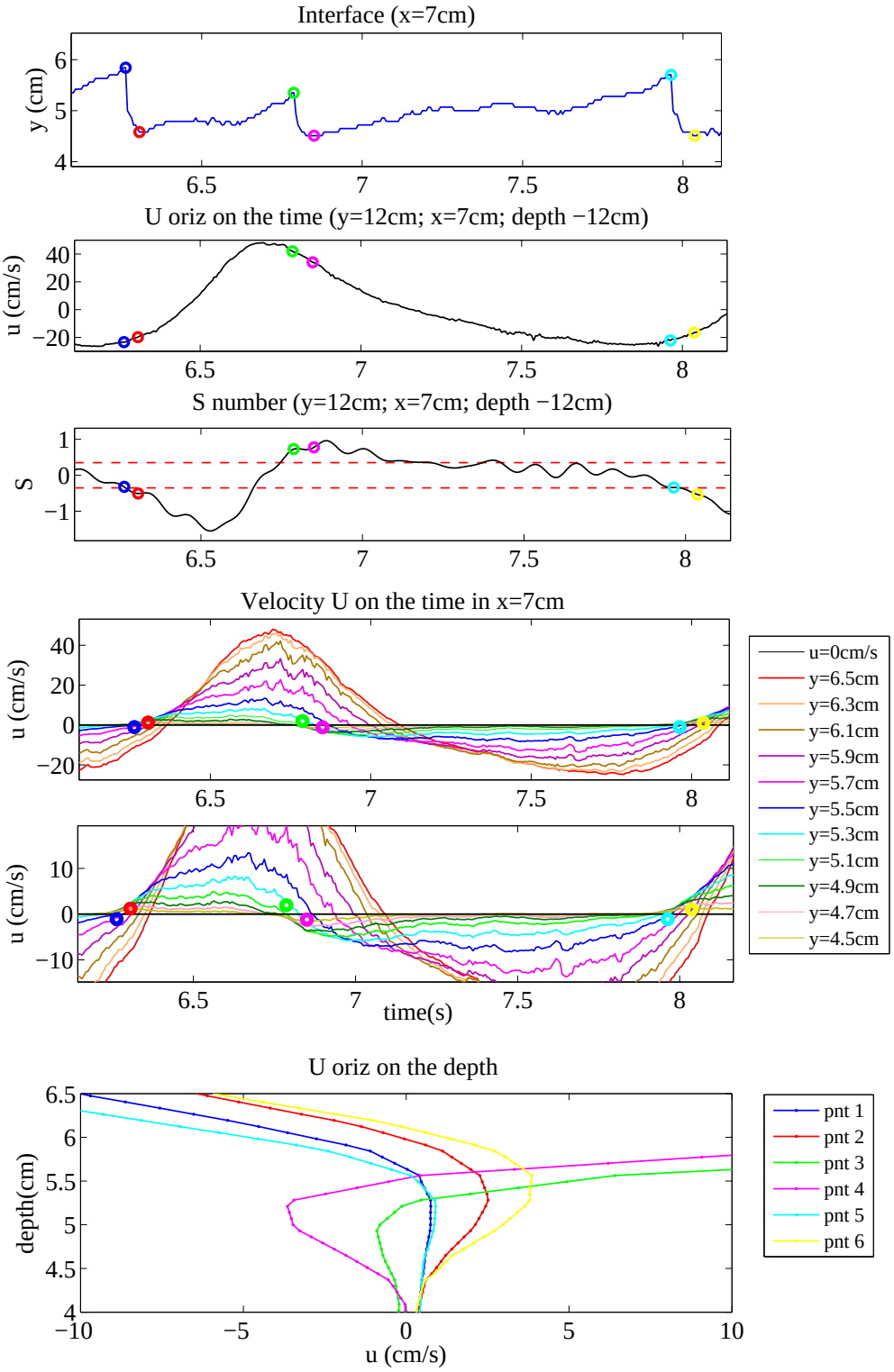

Figure 4.14. Analysis plug flow in t=[6,263; 6,306; 6,787; 6,85; 7,963; 8,037] s

Figure 4.14 show what it was explained before: It is recalled that the interface profile is suffering from an experimental criterion, it was chosen a speed threshold that seems the most appropriate, the information given on of the depth to which the plug flow occurs is relative. The error committed is minimal and so it is a good approximation, but do not be alarmed if these values do not correspond with those obtained from other graphics.

It must proceed as follows:

- from the graph of interface it identify the instants at which occurs the plug flow and the relative depth of the layers that form it;
- from the graph of the S number it check if the times are correct;
- from the graph of the time series of horizontal velocity in different depth it control if the depth of the layers, that form the plug flow, overlap;
- finally it look at the graph of horizontal velocity along the vertical if all data are correct.

Looking at the graph of horizontal speeds along the vertical can be identified the two profiles corresponding to the times of start and end of the plug flow. The two profiles intersect each other in the inflection point which determines the deepest layer up to which occurs exceeding the speed such as to generate movement of the grains during the instants of plug flow. From the point of inflection therefore it can determine the minimum speed for the movement in these wave conditions, and then tracing the vertical corresponding to this velocity, it can locate the intersection with the profile of the instant of beginning. This point identifies the upper layer of the plug flow and then it can be calculated the thickness of the plug flow. This

thickness compared with that obtainable from the graph of the interface appears to be concordant. Furthermore, it should deepen another concept. A result of having calculated the limits of S number as an approximation, is the fact that the instants of start and end of the plug flow in the graph of S number does not always correspond to the moments when there is start and end of the overrun of the limits. In this first analysis it is important that these points have a greater number S of the limits and this happens as seen in Figure 4.14.

4.1.6 Additional results

In this subsection it was analyzed all the information gathered for the spatial coordinate $x = 7cm$. The Figure 4.15 represents a time period of the first wave packet and reports the following graphs:

- Horizontal velocity calculated along the depth and function of time;
- Divergence and curl of velocity calculated along the depth and function of time;
- S number;
- Time series of horizontal velocity calculated in different depths.

Observing the graph of the horizontal velocity U, it is known that in a few moments the velocity quickly changes from positive to negative and vice versa. These abrupt changes are located in correspondence of the points where begins the phenomenon of plug flow because there are points where the flow reverses. Looking at the graph of the divergence it may be noted a difference: at the points in which it begins the phenomenon of plug flow, there are areas in which the value of the divergence is positive.

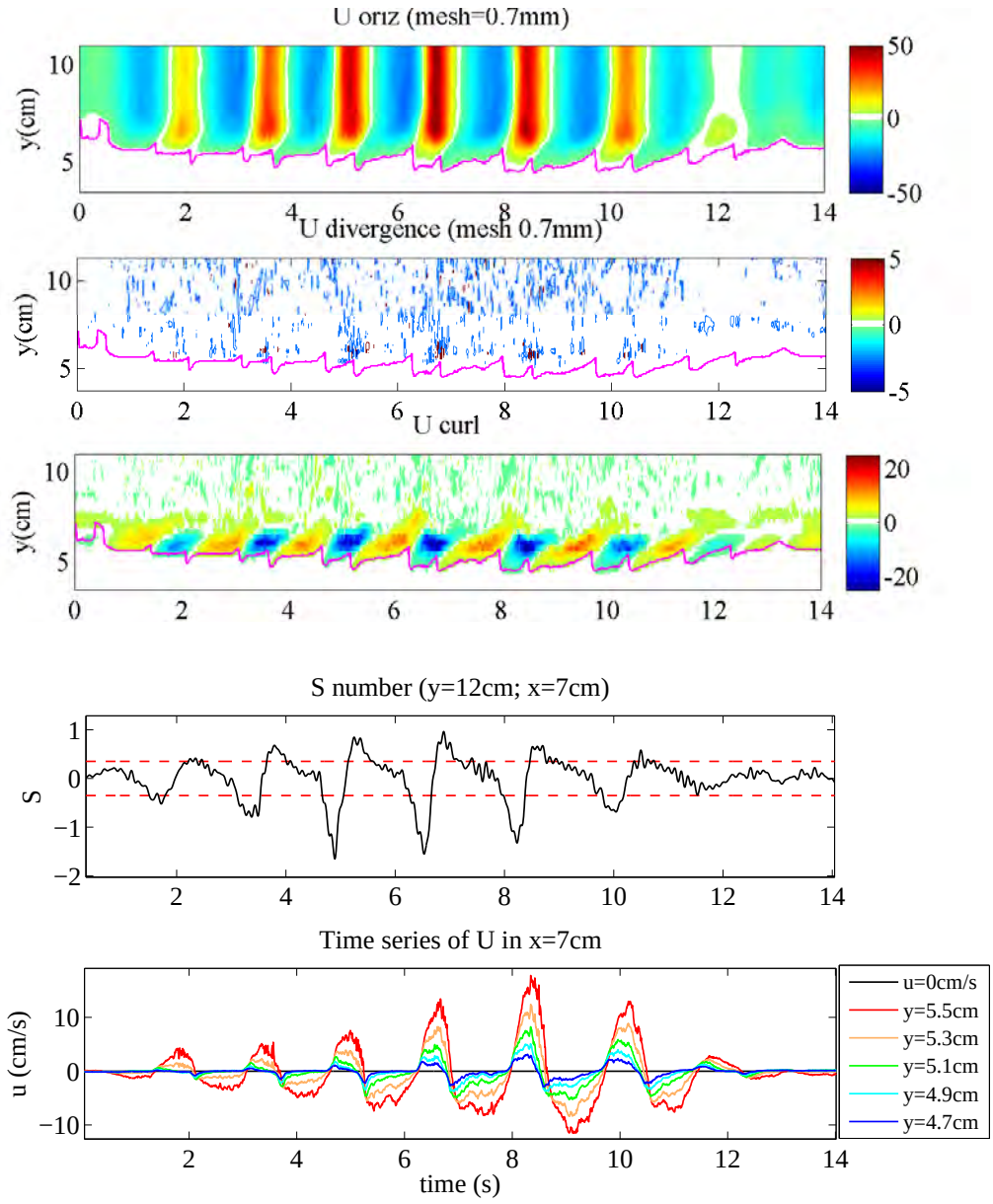

Figure 4.15. Analysis of dynamics in a packet of waves with mesh 0.7mm

The divergence is related to the concept of dilatancy of the particles in the layers, and then these particular points, in which the divergence is positive, indicate that there is a lower concentration, so it is more easy the motion of particles that allows the plug flow formation. Looking the graph of curl it can be understood many things. Moving from the crest to the through and examining the vertical at a point where there is a plug flow, it can see that in the upper layers in which the plug flow starts, there are negative curl and positive velocity while in the lower layers there are positive curl and negative velocity. This is explained by the fact that along the vertical approaching the bed, the velocity profile is decreasing, and then the upper layers are moved faster than the lower thus creating the vortex. So when the velocity is positive the curl has clockwise direction and therefore negative value when the velocity is negative the curl has anticlockwise direction and then positive value.

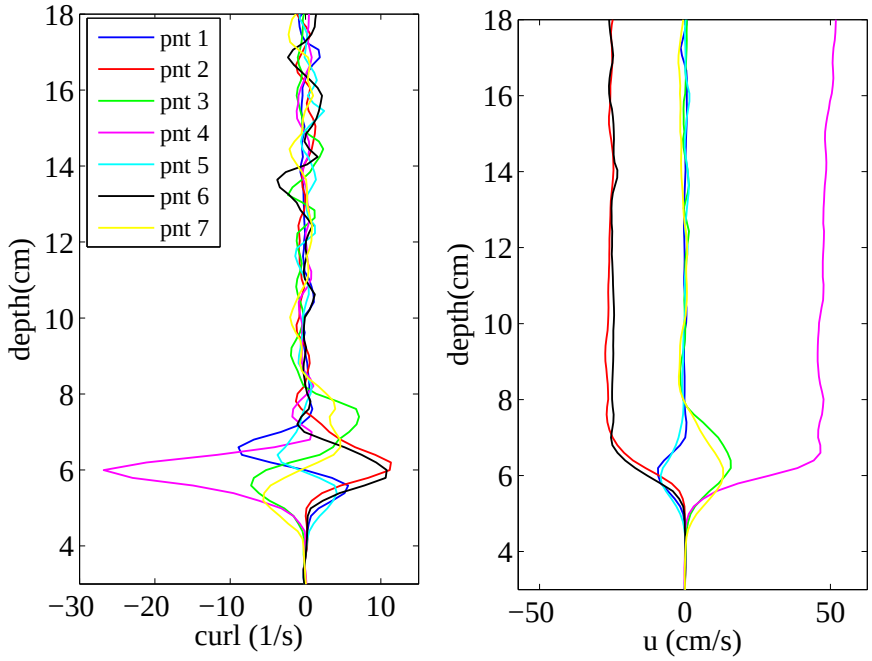

Figure 4.16. Relation between curl on vertical and velocity U on vertical (x=7cm)

This is observable in the Figure 4.16: considering the pink line corresponding to the crest of the wave, it can be seen what it was explained. The graph of the S number and the graph of the time series of U in different depth show the behaviour of the bed during the passage of the first wave packet.

4.2 Local analysis: 2^{nd} Experiment

TO BETTER study the phenomenon of the plug flow has been decided to focus the study on a part of the study area of the first experiment. Initially it was identified the interface between the particles in motion and static ones, then it was determined the thickness of the sheet flow that consists in the zone in which the particles move in suspension or by dragging on the seabed.

Later it was considered the model of Sleath taking as an example two plug flow of different nature and it was concluded that in these experiments require additional measurements in order to use this model.

Finally it found a good method based on exceeding the S number to identify when the plug flow occurs and how much erosion can cause.

4.2.1 Analysis of a section on time and identification of the interface

THE AIM of this subsection is to study a specific area of each image and see what happens over time. It was chosen a region of a width equal to the size of a grain and which extends for the whole height of the image, then it was made the average in the horizontal direction and so it was get an image that describes what happens in this region over time (Figure 4.17).

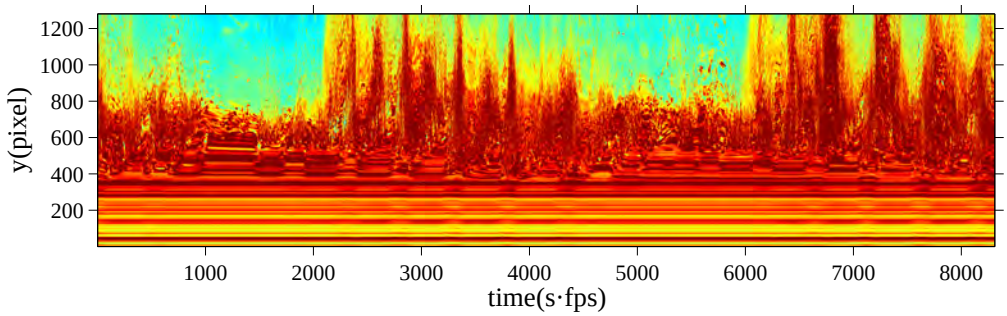

Figure 4.17. Section x = 2.35cm on time

From the image it can guess where is located the interface between particles moving and static particles. The objective is to calculate the interface and compare it with what it can see in the image of Figure 4.17. Then it is calculated the interface relatively to different velocity thresholds: 1cm/s; 0,8 cm/s and 0,7cm/s. It notes that calculated interfaces are very similar to each other and agree well with the image (Figure 4.18, Figure 4.19 and Figure 4.20).

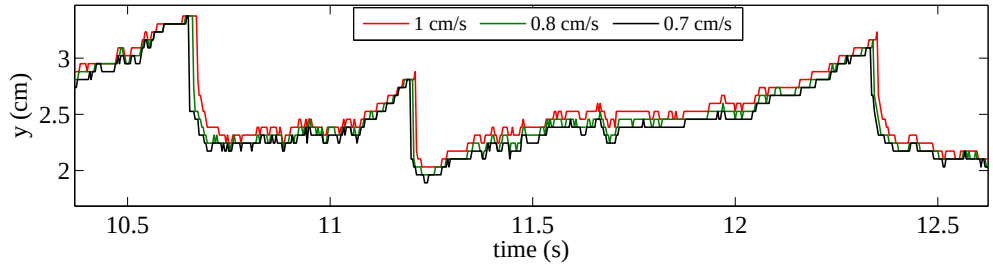

Figure 4.18. Interface with different thresholds of velocity U: 1 cm/s, 0.8cm/s and 0.7cm/s (x=2.35cm)

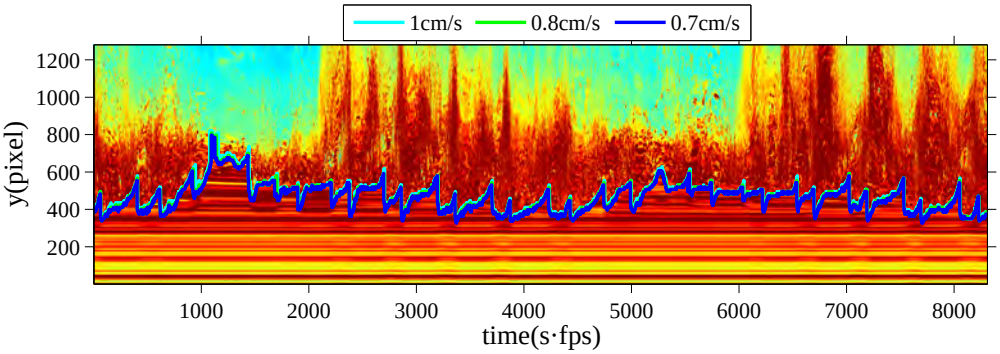

Figure 4.19. Section x = 2.35cm on time and 3 different interfaces

Very interesting it is to observe the behaviour of the gradient in the horizontal direction (Figure 4.21). First of all it can be noticed that the calculated interface agrees with the interface present in the image of the gradient. Also looking carefully, in the zoom of image (Figure 4.21 c), near the phenomenon of plug flow it can be seen areas where the gradient describes lines that tend upwards or downwards.

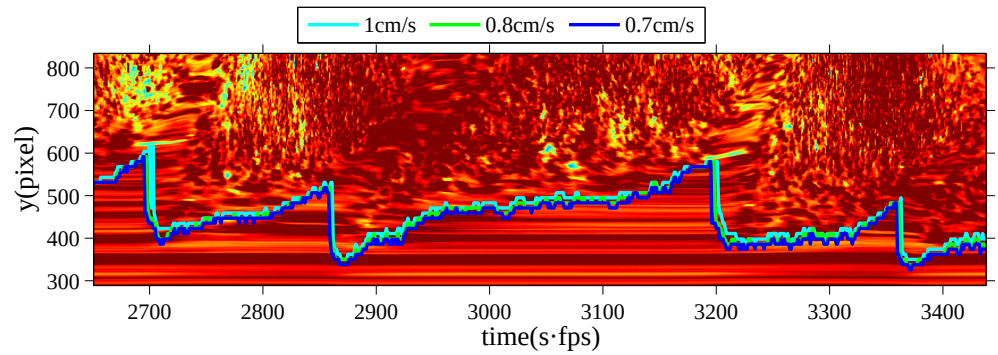

Figure 4.20. Zoom of section x = 2.35cm on time and 3 different interfaces

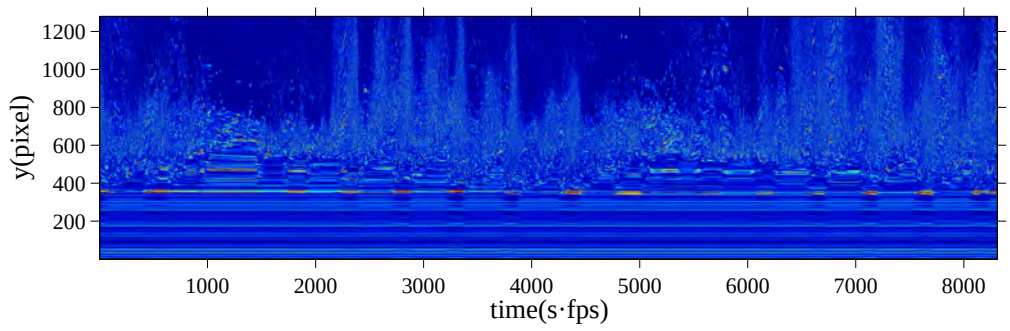

(a)

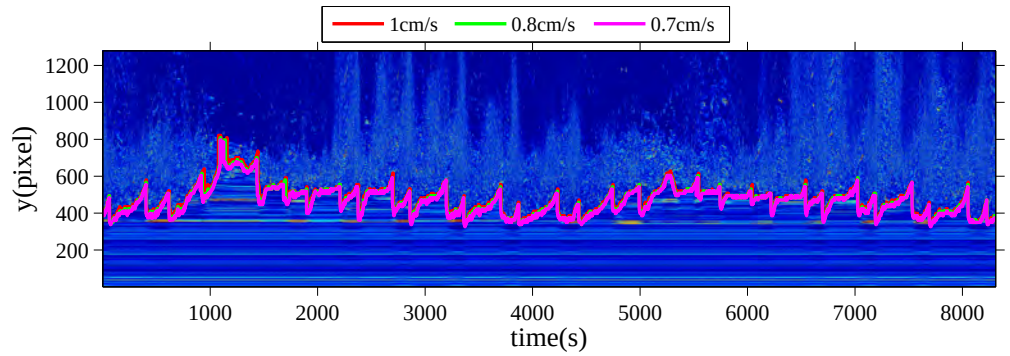

(b)

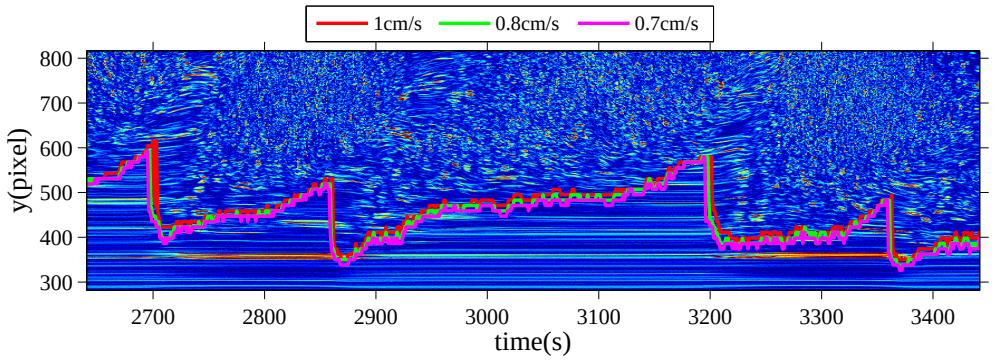

(c)

Figure 4.21. (a) Gradient of velocity U in x=2.35cm on time; (b) Gradient of velocity U in x=2.35cm on time and 3 different interfaces; (c) Zoom of gradient of velocity U in x=2.35cm on time and 3 different interfaces

Probably this happens because it is located in an area where the velocity change rapidly, and then the pressures: when the lines tend upwards means that the pressure in the bed is higher than that in the external fluid, and then the particles are pushed upwards; conversely for the lines down.

4.2.2 Additional results

In this second experiment there is the hope to obtain more detailed and precise information through the enlargement of a part of the area of study of the previous experiment. The study section is positioned at the coordinate x = 2,35 cm, which corresponds to the coordinate 22,85 cm in the reference system of the previous experiment. In this section, the share of the bottom is -16.71 cm respect the free surface and it corresponds to the depth y = 3.5 cm.

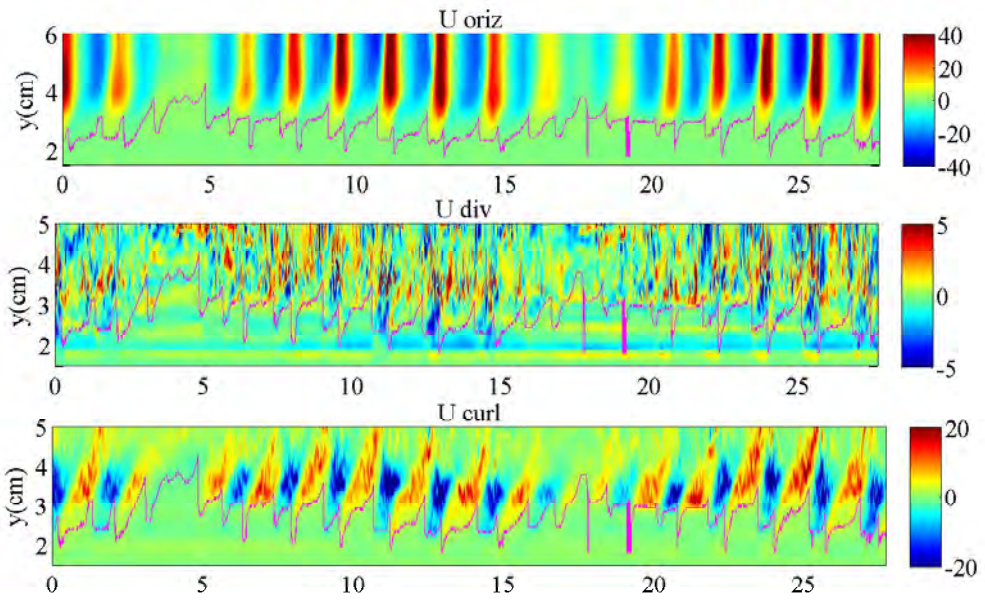

Figure 4.22. Analysis of dynamics in all time points with mesh 0.7mm

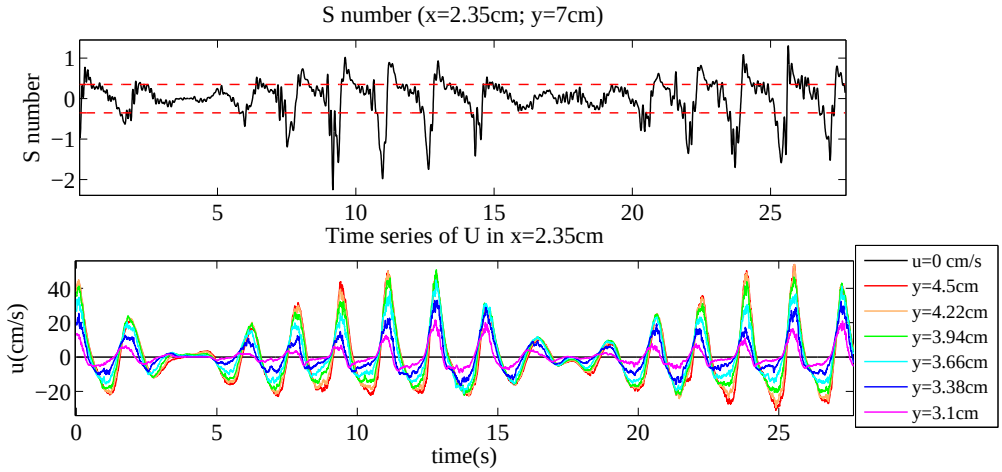

Figure 4.23. Analysis of dynamics in all time points with mesh 0.7mm

Figure 4.22 and Figure 4.23 show the graphs of horizontal velocity curl, divergence, S number and time series of horizontal velocity in different level of the bed. To calculate the S number is required acceleration at the free surface or very far from the bed. Hence it was considered that the acceleration in y = 7cm, or to 3,5cm above the level of the bed, is far enough away from the bed level, and then assimilable to those on the free surface. Indeed looking at the profile of horizontal velocity along the vertical (Figure 4.31) can be seen that the value is approximately that of the velocity on the free surface. These data appear to be consistent with the results of the previous experiment, but unfortunately the results do not improve.

4.2.3 Thickness of Sheet flow

THIS SUBSECTION is aimed to finding, if it is possible, the thickness of sheet flow. The thickness of sheet flow is obtained from the difference between the upper interface, which separates the transport zones of the sediments and the only current, and the bottom interface that separates the particles in motion by the particles still. Considering the image formed by the succession in time of a small region of the images and doing the

moving average, it can get the picture in Figure 4.24. Overlapping the interface between the particles static and in motion (solid black line), it can be seen that the results are consistent with each other, and this validate the results of bottom interface. Subjectively it was identified visually a value in the image that describe a plausible upper interface and so it was get the second interface (dashed black line). Therefore the area between the two interfaces represents the sheet flow and its thickness is the difference between them.

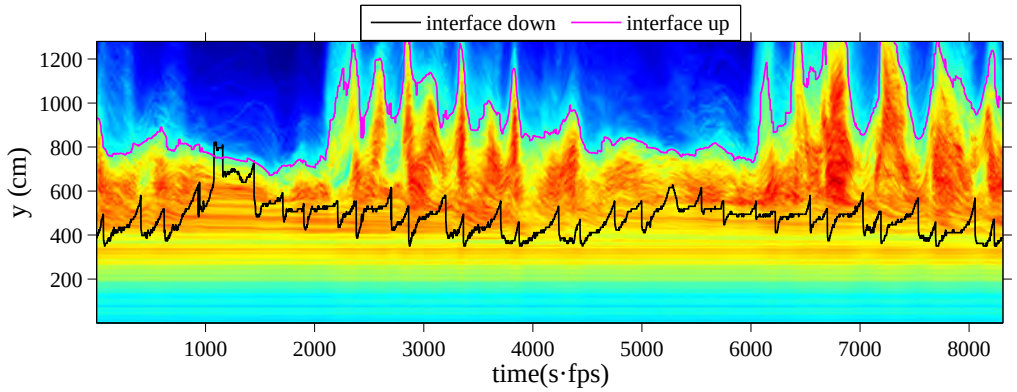

Figure 4.24. Section x = 2.35cm on time with bottom interface and sheet flow interface

To check if the results are confirmed it was overlapped the two interfaces to the image of gradient and, as it can be seen in Figure 4.25, the results are good.

Figure 4.27 to Figure 4.30 show the 2 interfaces, the thickness and their relatively zoom. Unfortunately this is not only the thickness of the sheet flow, but also includes a cloud of particles caused by the gravity current. Every time in which a wave packet is ending and then beginning the next wave packet, the gravity current brings back part of the particles moved previously by the wave packet. This causes a big mistake if it thinks that the contribution of sediment due to the cloud of particles is negligible. As it can be seen in Figure 4.27-4.30, in correspondence of the end of the first

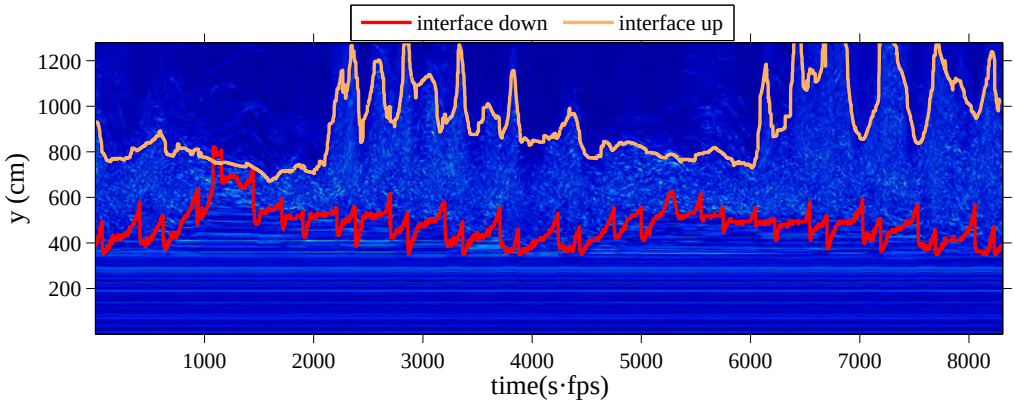

Figure 4.25. Gradient of velocity U in x=2.35cm on time with bottom interface and sheet flow interface

wave packet the sheet flow should have zero thickness but instead is of a few *cm*. Another verification can be done, is to consider the heights of the free surface detected by the gauge during the experiment. If the results are good it must be verified that during each crest the upper interface of the sheet flow presents a peak, and it can be seen in Figure 4.26 that this happens. There are also some imprecision due to the instruments. In fact there are some peaks that are cut on the top and this is because of the limited size of camera. Moreover, the position of free surface in the this figure is not at the correct depth, but it is moved down because of visualization problem.

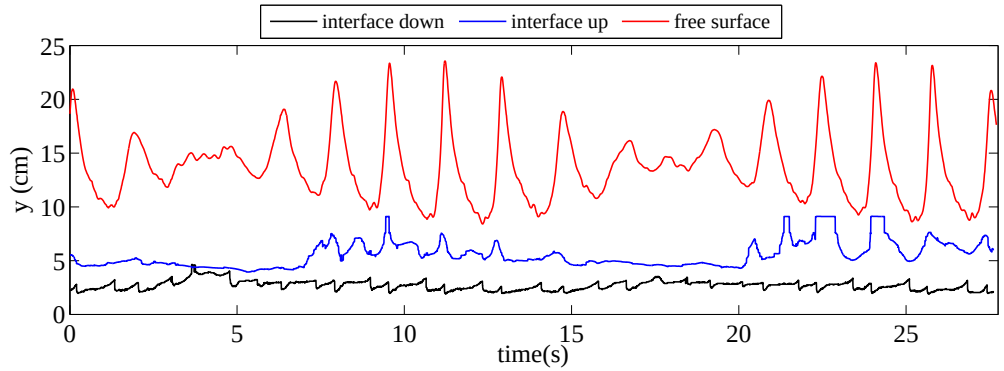

Figure 4.26. Bottom interface, sheet flow interface and free surface (x=2.35cm);

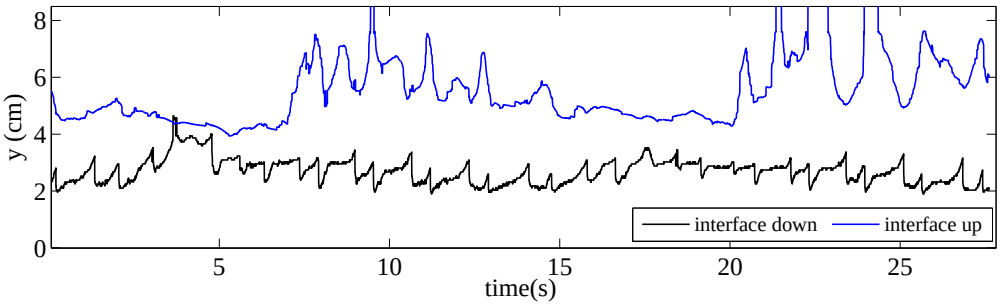

Figure 4.27. Sheet flow: bottom interface and sheet flow interface (x=2.35cm)

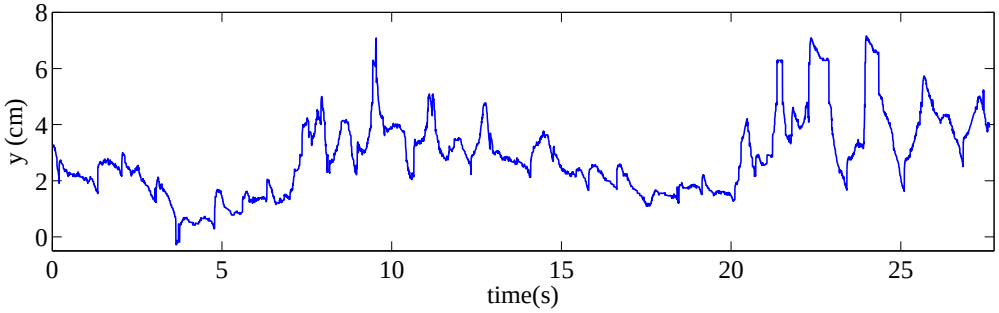

Figure 4.28. Thickness of sheet flow (x=2.35cm)

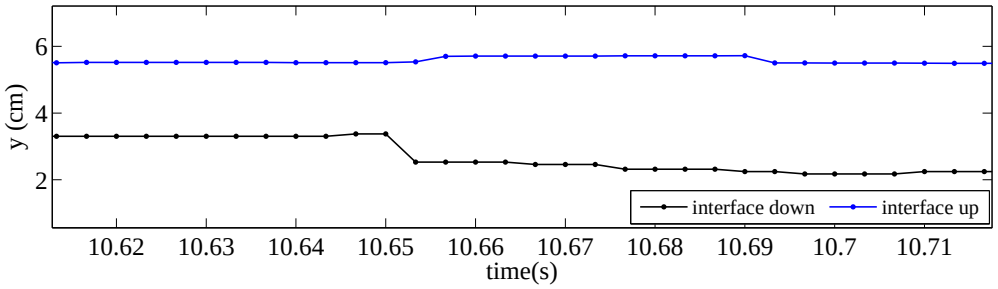

Figure 4.29. Zoom of Sheet flow: bottom interface and sheet flow interface (x=2.35cm)

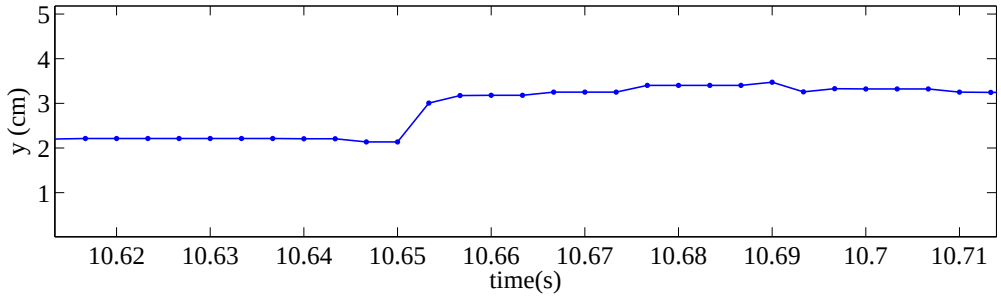

Figure 4.30. Zoom of Thickness of sheet flow (x=2.35cm)

4.2.4 Analysis of a plug flow

IT WAS ANALYZED the period of wave where there is the highest crest and it was observed the parts where are formed the plug flow. It was get results that agree with those of the previous experiment (Figure 4.31).

In this part of the analysis it wants to study the phenomenon of the plug flow more in detail. Chosen the plug flow that forms around the time $10.67s$, it was described the profile of each point between the start and the end of this plug flow. As it can be seen in Figure 4.32, the profiles that are formed over time pass from blue profile to red profile and all profiles included between them have a very particular shape.

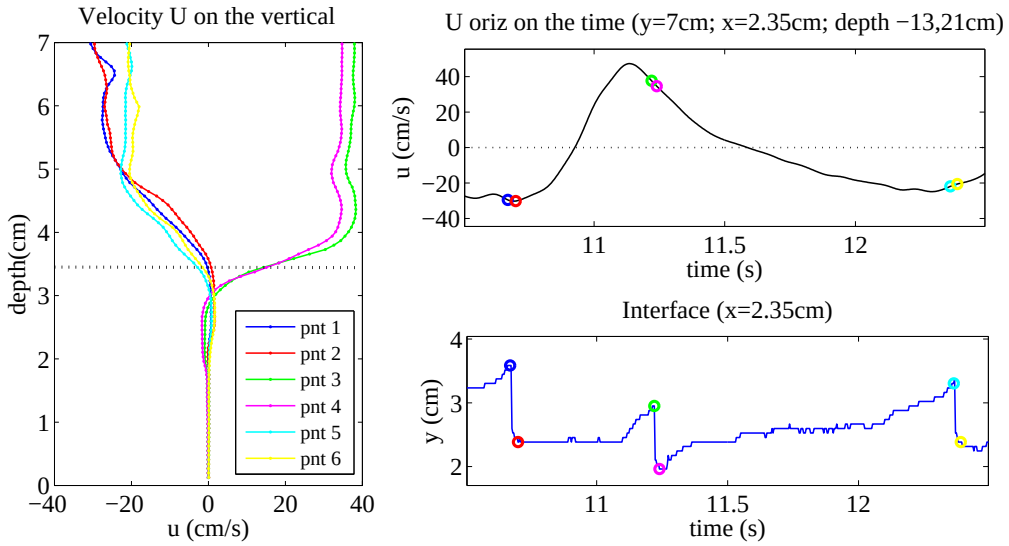

Figure 4.31. Analysis plug flow on 1 wave period in t=[10,67; 10,70; 11,22; 11,24; 12,36; 12,39] s

This shape is typical of the plug flow that is formed with the passage of the horizontal velocity U from negative to positive in a few instants. To notice is how the profiles are all parallel to each other until the point of inflection, in which all the profiles intersect, determining the deepest layer up to which occurs exceeding the speed such as to generate movement of the grains during the instants of plug flow. From the point of inflection

therefore it can determine the minimum speed for the movement in these wave conditions, and then tracing the vertical corresponding to this velocity, it can locate the intersection with the profile of the instant of beginning. This point identifies the upper layer of the plug flow and then it can be calculated the thickness of the plug flow. In the next section this argument will be discuss more in detail.

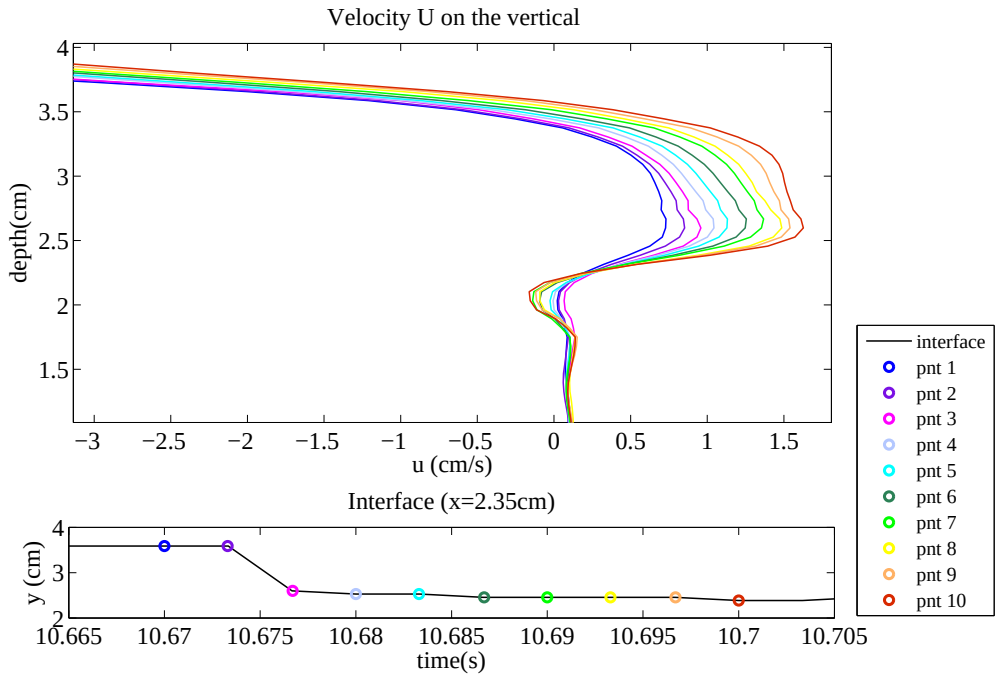

Figure 4.32. Profiles of all points of a plug flow in t=[10,6713; 10,6746; 10,678; 10,6813; 10,6846; 10,688; 10,6913; 10,6946; 10,6980; 10,7013] s

4.2.5 Sleath model

THE AIM of this subsection is to describe 2 application of the model of Sleath and so discover the value of the shear stress that causes the plug flow. As seen previously, the shear stress is calculated using the formula: $\tau = -\rho\tilde{u}\tilde{v}$ where $\tilde{u}$ and $\tilde{v}$ are the oscillating parts of the speeds respectively horizontal and vertical and it is compared with the shear stress obtained from the model according to Equation 2.11. A new term to con-

sider is the pressure. During the experiment the pressure is measured at 3 points along the vertical at distance $1.5cm$ each other. As it can be seen from Figure 4.33, $p1$ indicates the pressure at the lowest point, $p2$ is the pressure in the intermediate point and $p3$ is the pressure at the point closest to the interface.

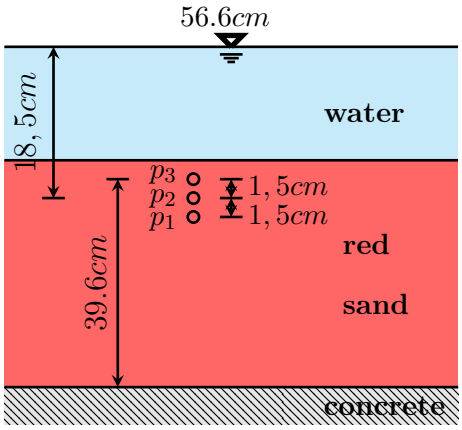

Figure 4.33. Position of pressure sensors

To calculate $\partial p'/\partial z$ it was taken the average of the two following configurations:

$$\left.\frac{\partial p}{\partial z}\right]_1 = \frac{p_2 - p_1}{\Delta z} \qquad and \qquad \left.\frac{\partial p}{\partial z}\right]_2 = \frac{p_3 - p_2}{\Delta z}$$

and then

$$\left.\frac{\partial p}{\partial z}\right]_{mean} = \frac{\left.\frac{\partial p}{\partial z}\right]_1 + \left.\frac{\partial p}{\partial z}\right]_2}{2} \tag{4.2}$$

Figure 4.34 represented the graph of $\partial p/\partial x$, the two configurations and the average of $\partial p/\partial z$.

One thing to keep in mind is the phenomenon of liquefaction, i.e. when the excess pore pressure is equal to the weight of the grains (the liquefaction criterion of *Mory et al. [2007]*):

$$\Delta P > \rho g d \left(\frac{\rho_s}{\rho}(1-n) + n \right) \tag{4.3}$$

with n is the porosity estimated equal to 0.5 and ΔP is positive for pressure gradient upwards. This criterion can be rewritten, using P_Z:

$$1 - P_Z > \frac{\rho_s}{\rho}(1-n) + n \tag{4.4}$$

With the characteristics of this experiment it was get that if $\partial p/\partial z]_{mean}$ exceeds the value 0.1 there is liquefaction. As it can be seen from Figure 4.34 where the green line indicates the limit of liquefaction, the $\partial p/\partial z]_{mean}$ not ever go over the limit and thus do not have the phenomenon of liquefaction but this line is still close enough to the curve to be able to think that the liquefaction participate in some way.

At this point it was studied the two plugs flow formed in a period in correspondence of maximum crest. So the first plug flow is formed at about $10.61s$ just after the through, while the second plug flow is formed at about $11.15s$ just after the crest.

In Figure 4.35 in blue it is represented the profile of the horizontal velocity U at the level of $7cm$, while in black are presented the profiles of the horizontal velocity U in the levels of the bed that the two plugs have in common.

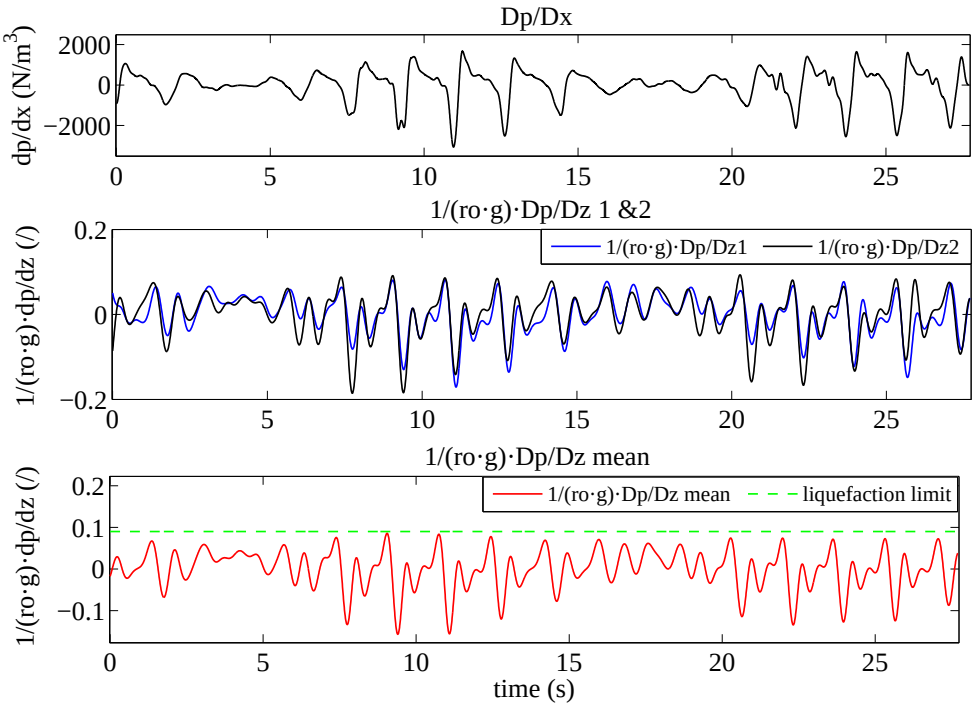

Figure 4.34. Analysis of pressure on vertical direction z and on horizontal direction x

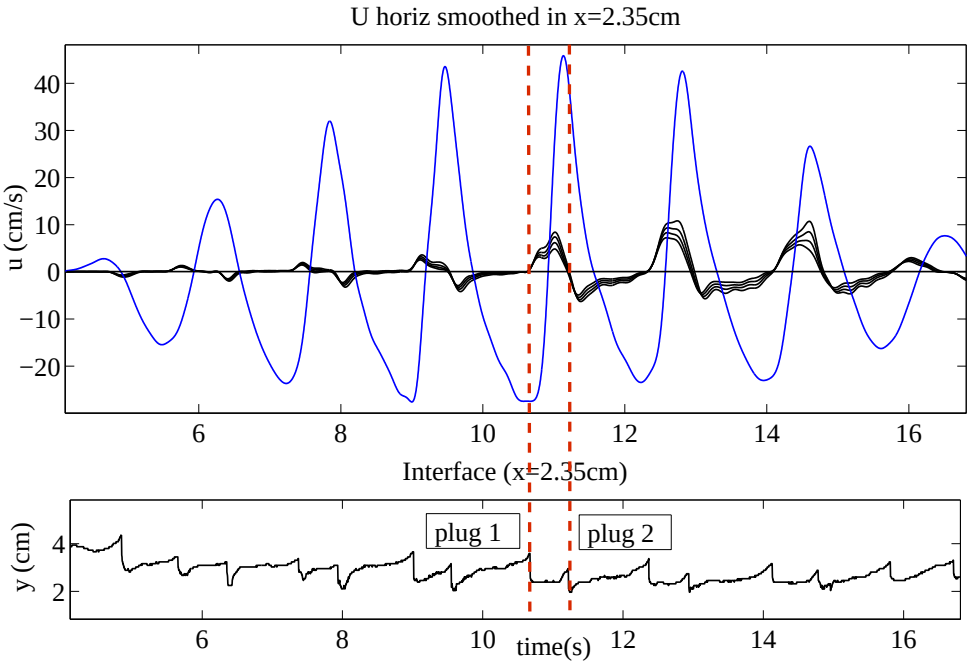

Figure 4.35. Choice of 2 plug flow: in t=10.67s and in t=11.15s

Plug1

TO BE NOTED are the particular conditions: the fluid has negative velocity, while at the same instants the bed is still under the influence of the positive velocity due to the through just passed (*phase lag*), then the profiles of horizontal velocity along the vertical are composed of two curves with opposite concavity. Observe more closely the phenomenon, focusing only what happens in the level of the bed. Figure 4.36 describes the sequence of steps of the formation of the plug in which each circle represents a grain.

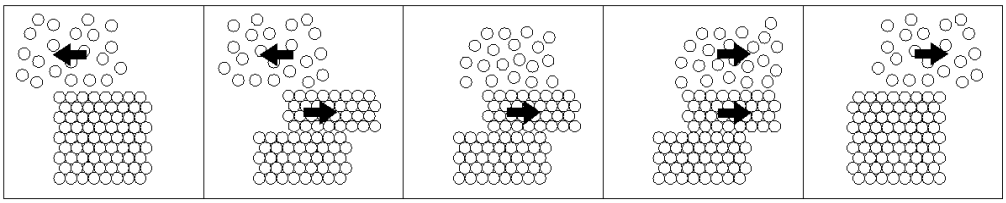

Figure 4.36. Sequences of formation of plug flow

The definition of plug flow is that for some instants there are a few layers of grains that move simultaneously, so it means that to find the deepest layer of grains in motion, it have to look for an inflection point for which pass all the profiles. The profiles are all parallel to each other until the point of inflection, in which all the profiles intersect, determining the deepest layer up to which occurs exceeding the speed such as to generate movement of the grains during the instants of plug flow. From the point of inflection therefore it can determine the minimum speed for the movement in these wave conditions, and then tracing the vertical corresponding to this velocity, it can locate the intersection with the profile of the instant of beginning. This point identifies the upper layer of the plug flow and then it can be calculated the thickness of the plug flow. In this case it has negative speed which decreases, resulting in a phase of deposit of sediment, which

later becomes positive, resulting in a phase of movement of sediments and therefore erosion. The profile outlined by the interface is determined by considering that the threshold speed for which they move the particles is $+/-1cm/s$.

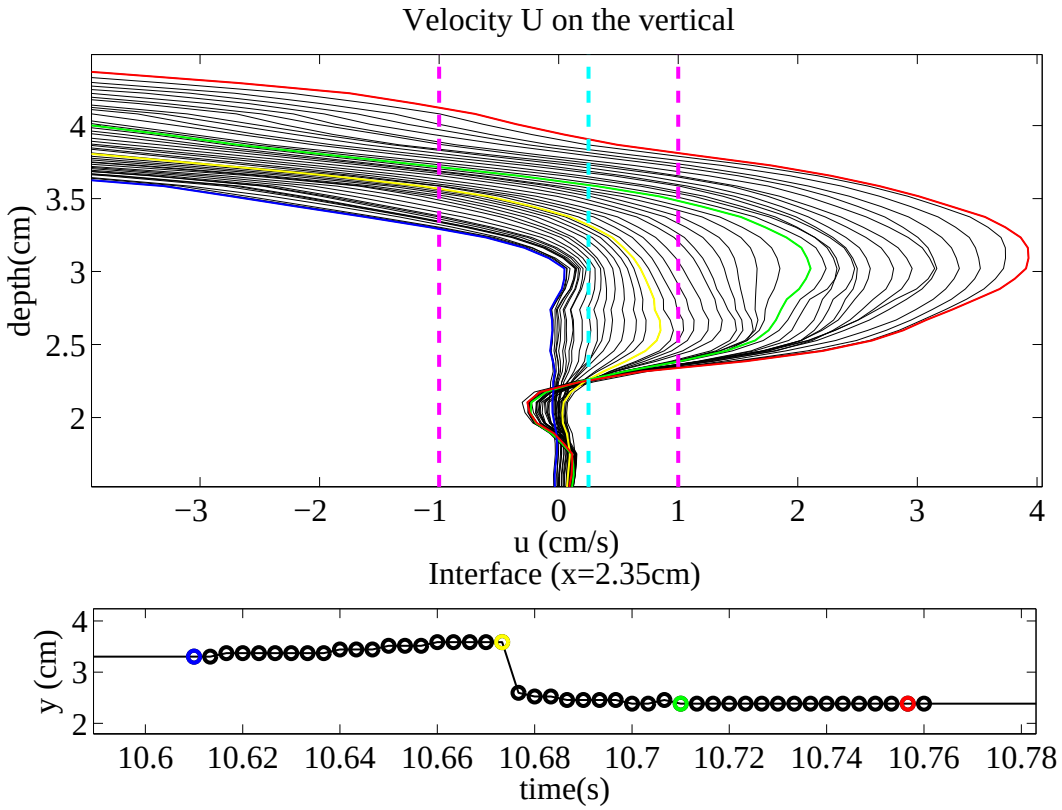

Figure 4.37. Profiles of velocity U on the vertical during the plug in t=10.67 s

In the graph of velocity (Figure 4.37) it is seen that this threshold is overestimated for the formation of plug flow and that the criterion explained before regarding the point of inflection is much more reasonable. So looking at the graph, it was identified the inflection point which is characterized by a velocity of $0.2493cm/s$, located at height $2.26cm$. To identify the instant in which is formed the plug flow, it must locate the first profile passing through the inflection point. In this case time runs progressively from left to right and then this profile corresponds to the yellow one. Regarding the instant

of end of plug flow, there are no definitions or rules that define it. Observing the experiment it is seen that with the passage of time the thickness of the plug flow expands upward and tends to decrease downward, and this is also understood by the trend speed profiles along the vertical. In this research, it fixed the instant of end of plug flow corresponding to the green profile. As each profile represents the velocity along the vertical at a certain instant, then all points with a velocity higher than that of the inflection point for each profile, which goes from the yellow to the green, represent layers of the grains in motion during plug flow. So it can be calculated the *thickness of the plug* for each instant by the difference between the inflection point, common to all the profiles, and the point that the profile intersects the cyan line that indicates the velocity limit for the plug flow.

Now it can consider the **model of Sleath**.

The following graphs in Figure 4.38 show all the data necessary to calculate the shear stress:

- $\frac{\partial p}{\partial z}\Big]_{mean}$, $\frac{\partial p}{\partial z}\Big]_{1}$, $\frac{\partial p}{\partial z}\Big]_{2}$;
- $\frac{\partial u_s}{\partial t}$ where u_s is the velocity in the layers that compose the plug flow, and then for each profile is an average value (red line) and a maximum value (blue line);
- $\frac{\partial p}{\partial x}$.

and the shear stress calculated as $\tau = -\rho\tilde{u}\tilde{v}$.

Regarding $\frac{\partial p}{\partial z}$ it can be seen that taking the average of the two curves it does not make a big mistake; however later, all three curves will be considered and so it can be seen if this negligible error is amplified or reduced. In the model it was considered the average value of $\frac{\partial u_s}{\partial t}$ even though is not much different from the maximum value, as shown by the graph.

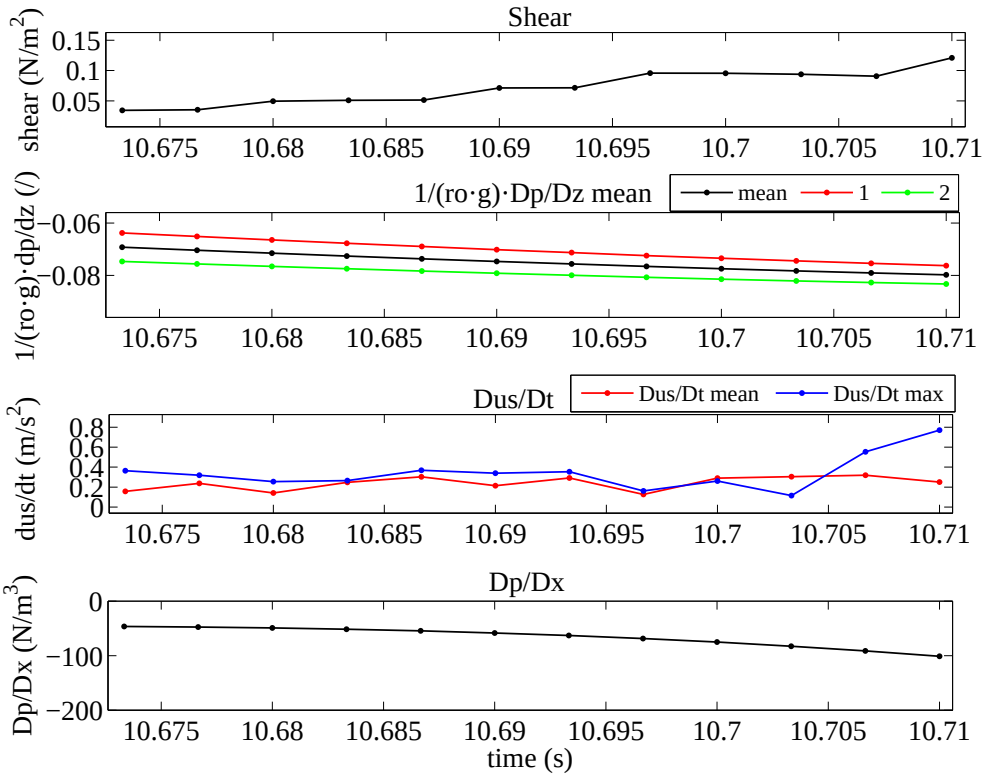

Figure 4.38. Analysis of the terms of the Sleath Equation in plug in t=10.67 s

Substituting these values in the model Sleath, it was got the shear stress and, as it was been used three different values of $\frac{\partial p}{\partial z}$, in the Figure 4.39 it can be seen three different colored lines. At first sight it is clear that the comparison between the three colored lines and the solution $\tau = -\rho\tilde{u}\tilde{v}$ (black line) is not good. The three colored lines are the values of the shear stress that it would need to obtain the thickness of the plug calculated by the graphical method validated by the video.

The values are too different and therefore could mean: there is an error in the model, perhaps there is another term to consider, or the shear stress calculated as $\tau = -\rho\tilde{u}\tilde{v}$ formed by velocities has something strange.

In fact in the graph of the thickness can be observed that the thickness calculated considering shear stress equal to $\tau = -\rho\tilde{u}\tilde{v}$ is definitely wrong if the comparison with the thickness derived from the graphical method

(experimental evidence as it is consistent with the video of the experiment).

To find a possible solution it was studied in detail the profiles of shear

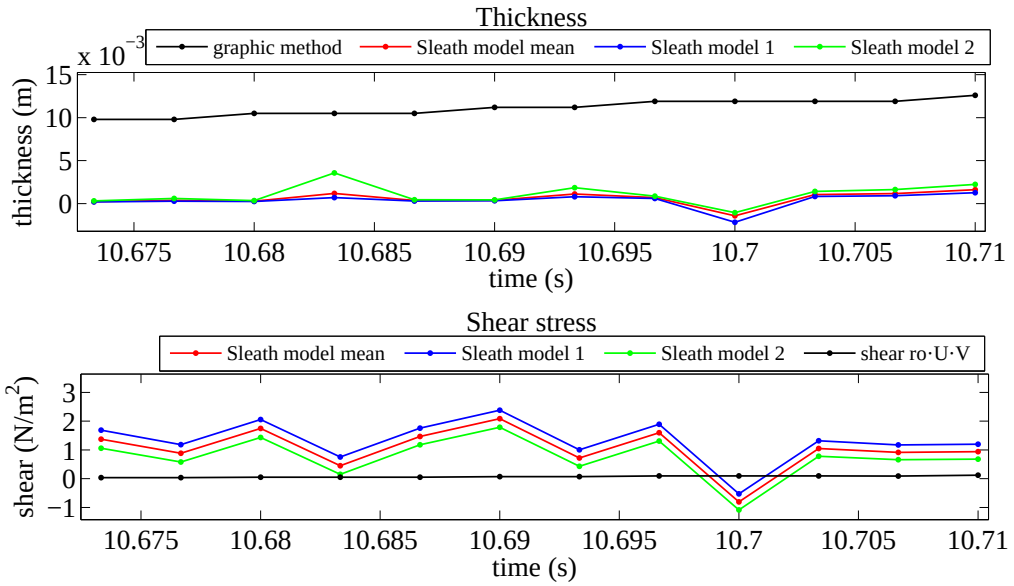

Figure 4.39. Comparison between different methods of calculation regarding thickness and shear stress in plug in t=10.67 s

stress, U and V. Zooming the interface at the point of plug flow considered, it was chosen to study the profiles of the shear stress in 4 different depths in order to consider: the lowest layer of the plug flow, the intermediate layer, the first layer that moves and a layer above the plug flow. As it can be seen from Figure 4.41, if it was considered to calculate the shear stress as $\tau = -\rho\tilde{u}\tilde{v}$, it was get that during the plug flow there are positive value in the layers above the first layer which moves, and negative values in the lower layers to this last. In the model the shear stress is related to the layer in motion of the plug flow, so considering $\tau = -\rho\tilde{u}\tilde{v}$ or considering the formula of Sleath model, it can obtain positive value of the shear stress. This, however, is in contrast with physical reality, because it expects a shear stress in the opposite direction compared to the velocity of plug flow and that are a negative values (Figure 4.40).

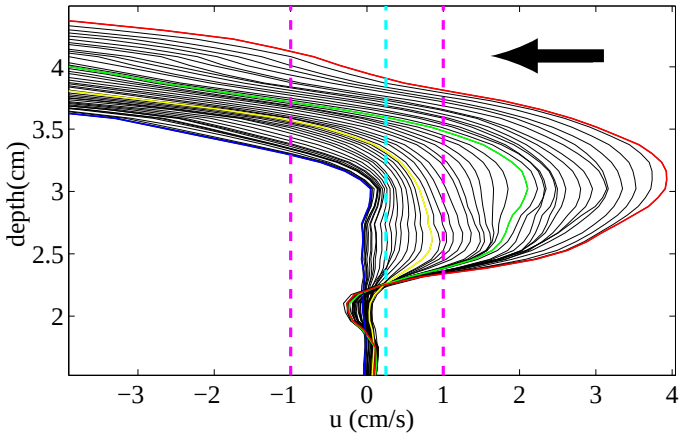

Figure 4.40. Correct direction of shear stress in plug in t=10.67 s

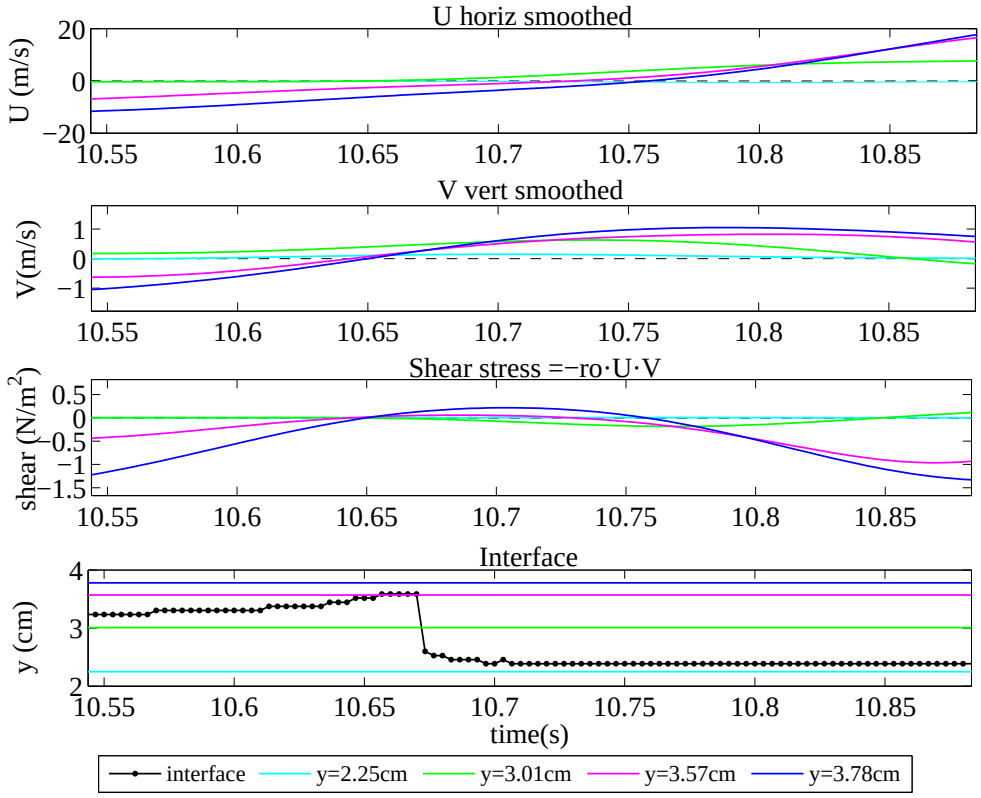

Figure 4.41. Analysis of shear stress in significant positions of bed in plug in t=10.67 s

Plug2

TO BE NOTED are the particular conditions: the fluid has positive velocity, while at the same instants the bed is still under the influence of the negative velocity due to the crest just passed (*phase lag*), then the profiles of horizontal velocity along the vertical are composed of two curves with opposite concavity. Observe more closely the phenomenon, focusing only what happens in the level of the bed. Figure 4.42 describes the sequence of steps of the formation of the plug in which each circle represents a grain.

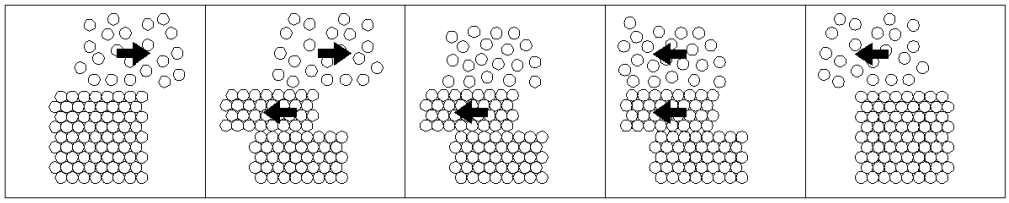

Figure 4.42. Sequences of formation of plug flow

To analyse the second plug flow it was used the same procedure to analyse the *plug1*. So looking at the Figure 4.43, it was identified the lower inflection point which is characterized by a velocity of $-0.5186 cm/s$, located at height $1.81 cm$ and it was calculated the thickness of the plug flow for each time.

So now it was shown the Figure 4.44 that represents the data used to calculate the shear stress according to the **model of Sleath** and the Figure 4.45 about the shear stress calculated as $\tau = -\rho\tilde{u}\tilde{v}$. As for *plug1*, it can do the same considerations on the components of the model of Sleath, but obviously the difference is that in this case $\frac{\partial p}{\partial x}$ is positive. Substituting these values in the model Sleath, it was got the shear stress and, as it was been used three different values of $\frac{\partial p}{\partial z}$, in the Figure 4.45 it can be seen three different colored lines. The three colored lines are the values of the shear

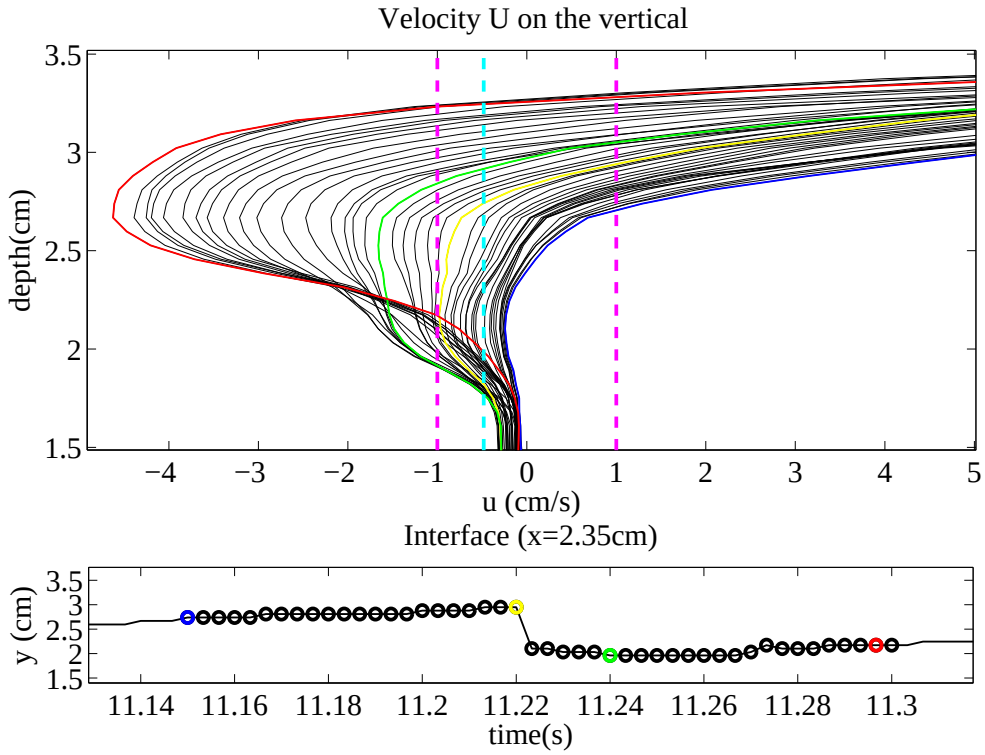

Figure 4.43. Profiles of velocity U on the vertical during the plug in t=11.15 s

stress that it would need to obtain the thickness of the plug calculated by the graphical method validated by the video. It is clear that the comparison between the three colored lines and the solution $\tau = -\rho\tilde{u}\tilde{v}$ (black line) is very bad: the values are 3 different orders of magnitude. In fact in the graph of the thickness can be observed that the thickness calculated considering shear stress equal to $\tau = -\rho\tilde{u}\tilde{v}$ is definitely wrong if the comparison with the thickness derived from the graphical method (experimental evidence as it is consistent with the video of the experiment).

So, to find a possible solution, it was studied in detail the profiles of shear stress, U and V. Zooming the interface at the point of plug considered, it was chosen to study the profiles of the shear stress in 4 different depths in order to consider: the lowest layer of the plug flow, the intermediate layer, the first layer that moves and a layer above the plug flow. As it can be

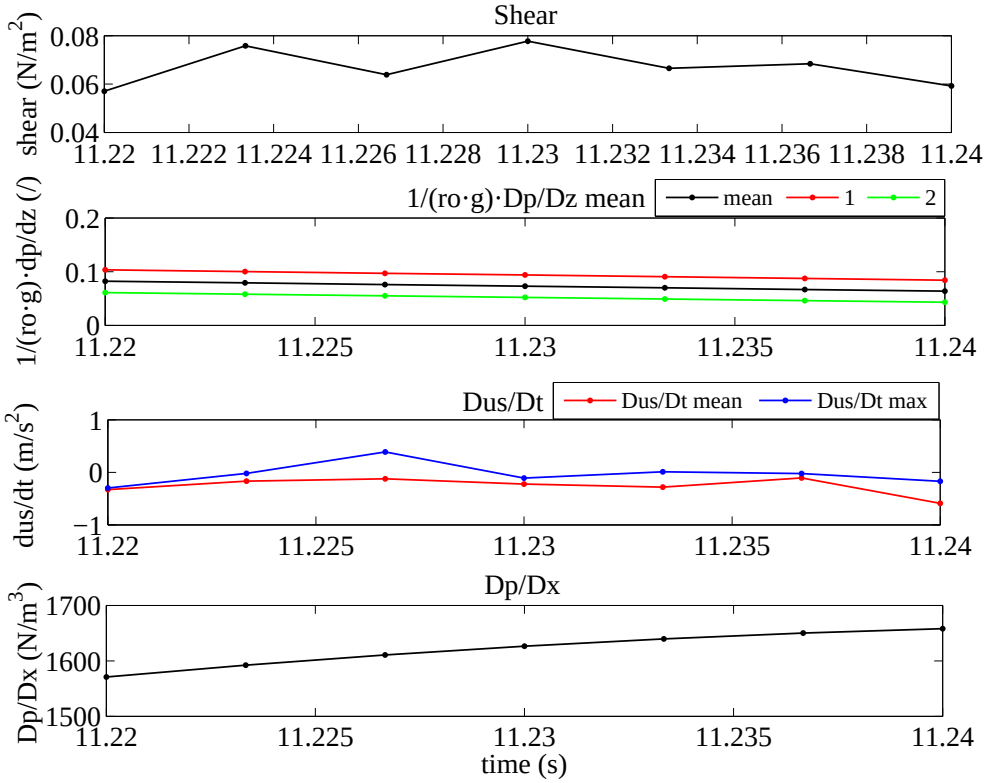

Figure 4.44. Analysis of the terms of the Sleath Equation in plug in t=11.15 s

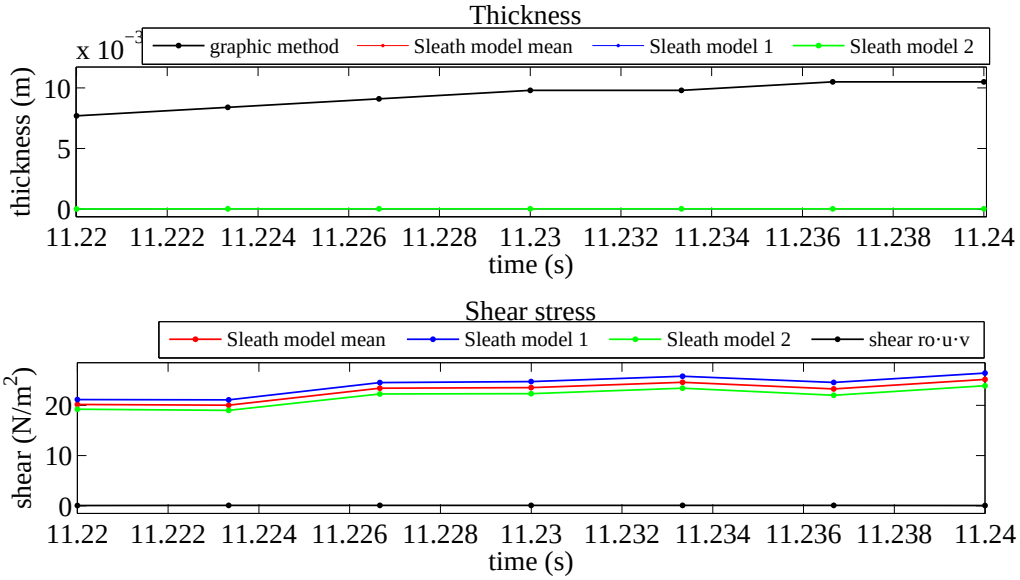

Figure 4.45. Comparison between different methods of calculation regarding thickness and shear stress in plug in t=11.15 s

seen from Figure 4.46, if it was considered to calculate the shear stress as $\tau = -\rho\tilde{u}\tilde{v}$, it was get that during the plug flow there are positive value in the layers above the first layer which moves, and small negative value in the lower layers to this last.

In the model the shear stress is related to the first layer in motion of the plug flow, so considering $\tau = -\rho\tilde{u}\tilde{v}$ or considering the formula of Sleath model, it can obtain positive value of the shear stress. This, however, is in agreement with physical reality, because it expects a shear stress in the same direction of the velocity of plug flow, but the values are much different (Figure 4.47).

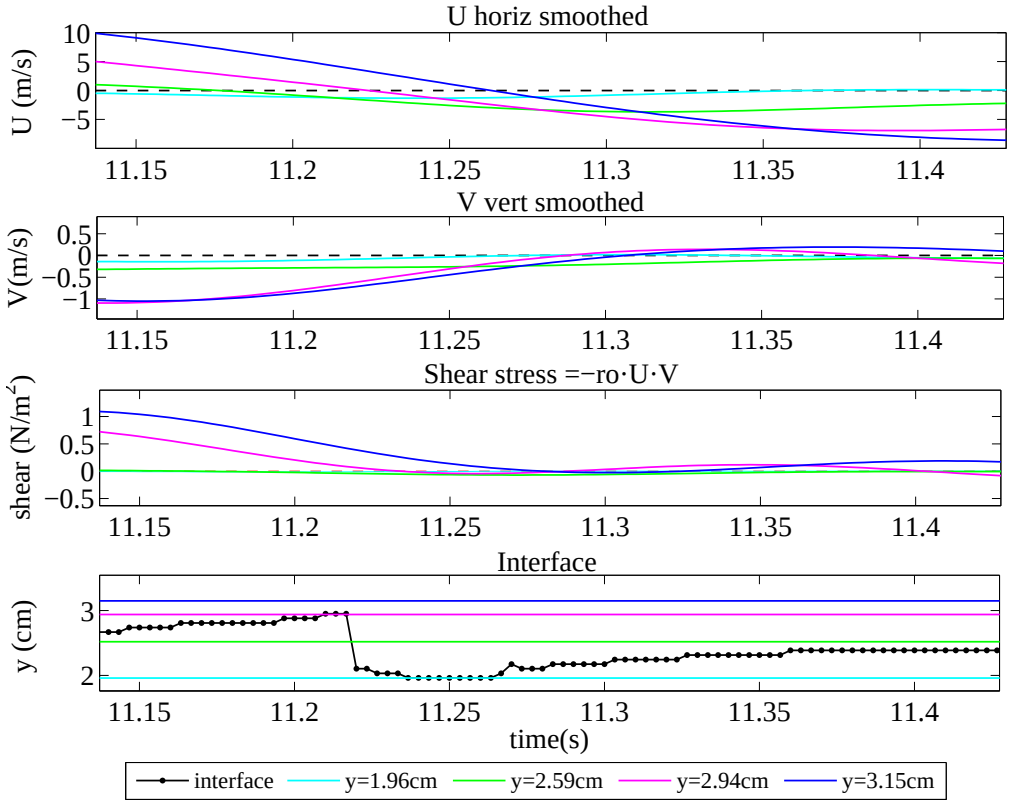

Figure 4.46. Analysis of shear stress in significant positions of bed in plug in t= 11.15s

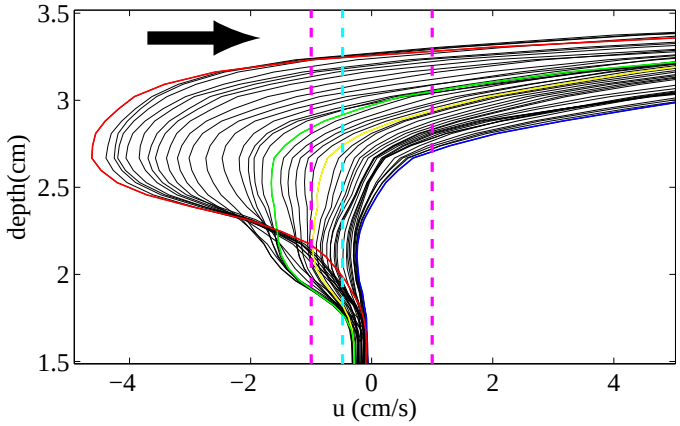

Figure 4.47. Correct direction of shear stress in plug in t= 11.15 s

4.2.6 Sleath number S

It was calculated S number and the limit to which it should have the plug flow when S exceeds this limit. It remembers that, according with Sleath, S number is:

$$S = \frac{-\rho \frac{\partial u_\infty}{\partial t}}{g\Delta\rho} = \frac{\frac{\partial p}{\partial x}}{g\Delta\rho} \tag{4.5}$$

which, as he explained in his article, it can be considered approximately equal to the $K_f C^*$, which for the majority of cases appears to be about $0.3 - 0.35$. In this model, because $\frac{d_{50}}{\delta_s}$ is very small, you can be considered S_{limit} equal to

$$|S_{limit}| = K_f \left(C^* + \frac{1}{g\Delta\rho} \frac{\partial p}{\partial z} \right) \tag{4.6}$$

In this case it is assumed that the concentration C^* is equal to 0.5 and that K_f is equal to 0.7, in order to have the first constant term equal to 0.35 as indicated by Sleath. Then it was get a limit of S that depends on the value of $\frac{1}{g\Delta\rho}\frac{\partial p}{\partial z}$, which is the value that identifies the liquefaction, and

therefore this value gives a great contribution to the formation of the plug flow.

In (Figure 4.48) it was been highlighted with grey rectangles the instants when S exceeds the limit, and it can be seen that this happens exactly at all plugs flow. To be noted is that the interface calculated by the velocity threshold equal to $1cm/s$ is not always so correct. In fact you can seen that the start times and end times of the plugs flow do not coincide with the times identified by the S number. This means that the layers need less or greater velocity to be moved, compared to the threshold value chosen.

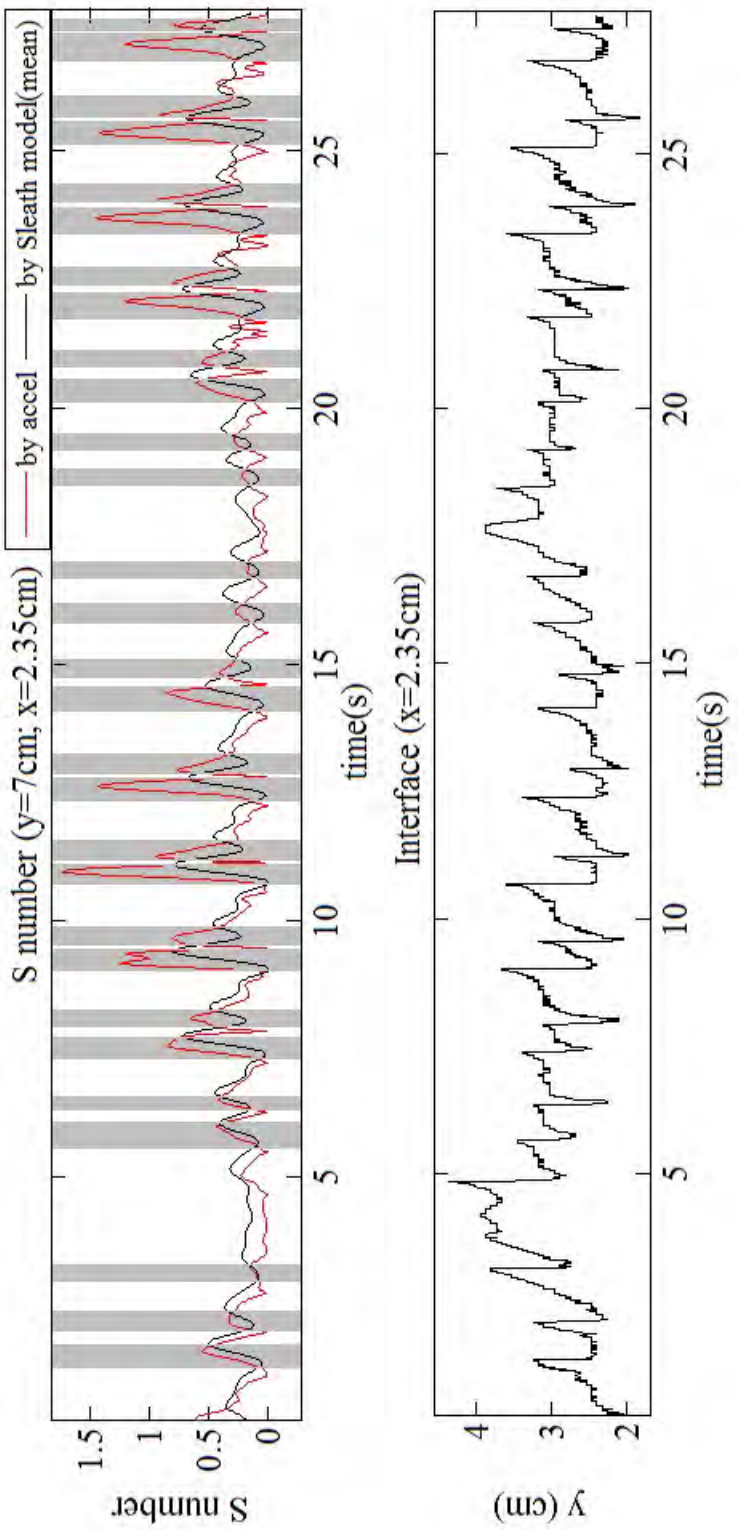

Figure 4.48. Analysis of S number and identification of exceedances of S limit that identify the plug flow formations

4.2.7 General validation of S number for global scale in the 1^{st} experiment

GIVEN that, this formula, in which it was also considered the term of pressure on the vertical, is very accurate, so it wants to check if it works also well in the previous case of the experiment in a global scale. By analyzing the pressures of the first experiment (Figure 4.49), it was calculated the mean pressure on the vertical and then it was calculated the new limit for S number. As it can be seen from Figure 4.50 and Figure 4.51, this method of calculation of the limit for S number is optimal and then now this formulation appears to have general validity and not only suitable for a local scale. As for the second experiment it was been highlighted with gray rectangles the instants when S number exceeds the limit, and it can be seen that this happens exactly at all plugs flow.

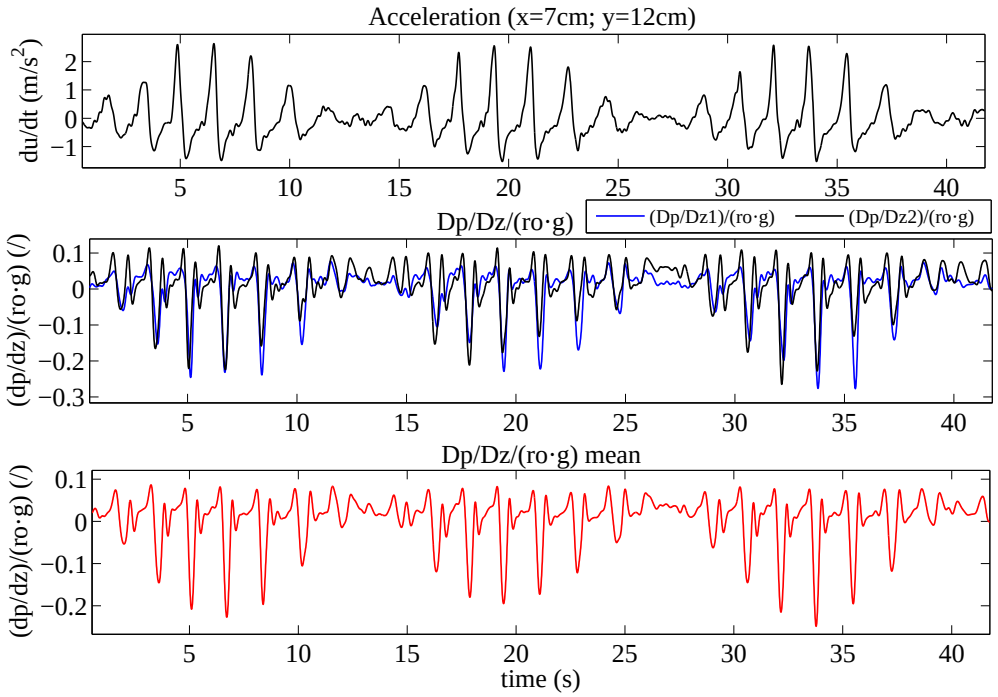

Figure 4.49. Analysis of acceleration and of pressure on vertical direction z

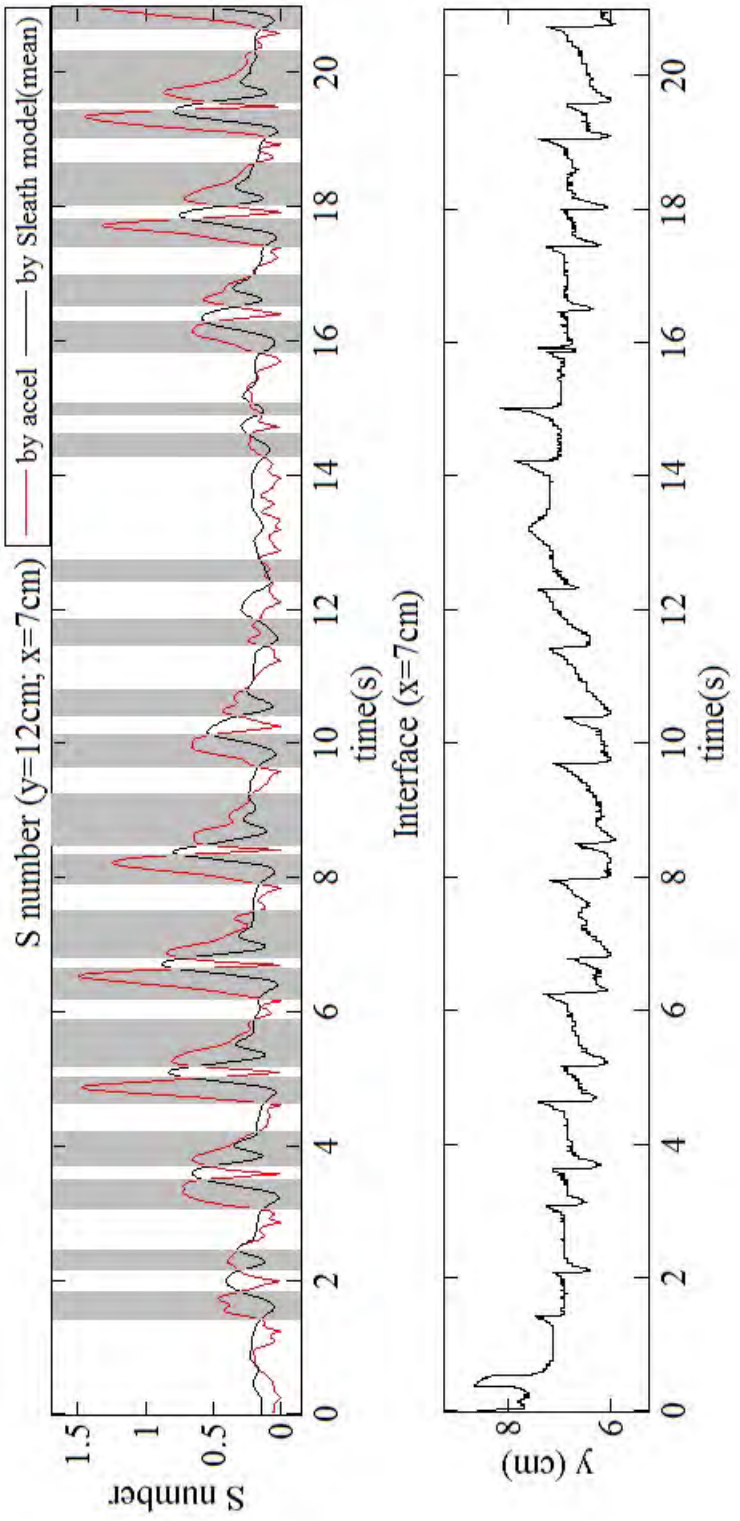

Figure 4.50. Analysis of S number and identification of exceedances of S limit that identify the plug flow formations in 1st experiment (t=0-21 s)

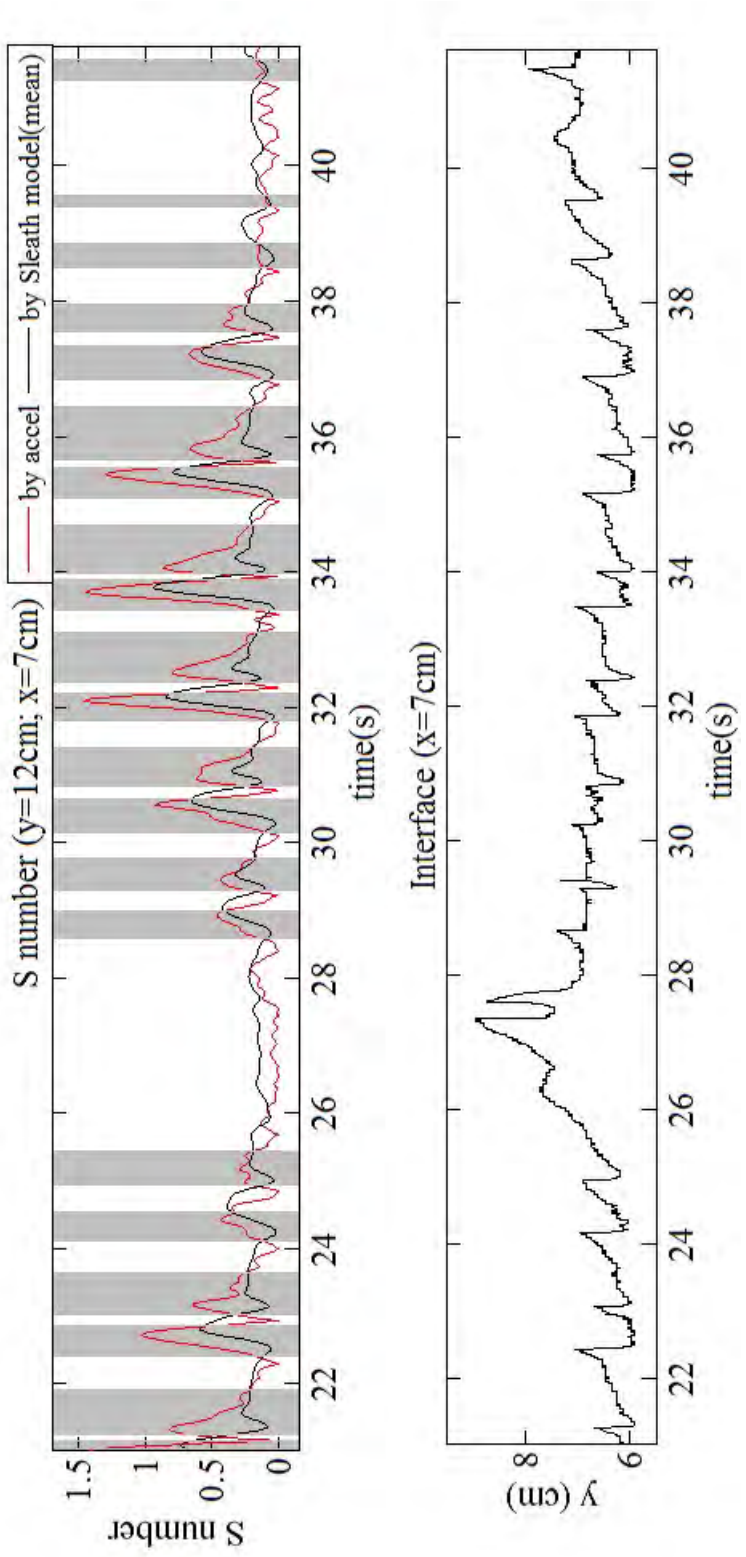

Figure 4.51. Analysis of S number and identification of exceedances of S limit that identify the plug flow formations in 1st experiment (t=21-41.75 s)

Chapter 5

Conclusion

In order to analyze the phenomenon of the formation of plug flow, it was initially studied in the first experiment the dynamics and characteristics of the phenomena on a global scale and then it was studied the phenomena on a local scale in the second experiment.

It was reached these conclusions:

1. Comparing the velocity profiles U along the vertical with those found by Nielsen, it was confirmed that the shapes of the profiles are in agreement and that the phenomenon of overshoot occurs at a small distance from the bottom.

2. To study the formation of plug flow is necessary to calculate Sleath number S and identify a limit value for which to identify the apparition of the phenomenon. In this study it is been assigned a value of 0.35. Also in the first experiment it was considered the value of S number constant in time and it depends only by the concentration of the particles, while in the second experiment the value of S number depends by the time because it also includes the term of pressure on

the vertical. Then to establish if it is good consider also the term pressure on the vertical, it is been applied the same formula used for the experiment in local scale to the experiment in a global scale. In fact it was obtained that the term is crucial for determining the value of S number and this is also visible in the figures. From Figure 4.50 and Figure 4.51, it can be seen that the term of pressure on the vertical has considerable importance, because only including it, it can get a very good correspondence between exceeding the limit of S number and formation of plug flow.

3. In agreement with Zala-Flores, the plug flow is formed when all velocity profiles U in different depths overlap for a few moments around a 10th of second. In fact when it happens it means that all those layers move simultaneously, and this is the definition of plug flow.

4. From Figure 4.31, it can be seen that the formation of plug flow occurs when there are strong accelerations in the profile of velocity U and therefore there is always a plug flow immediately after the trough and one immediately after the crest. From Figure 4.32, it can be seen the typical shape of the velocity profiles U in the layers units within the plug flow. To be noted is the typical shape of the velocity profiles U in the layers including the plug flow (Figure 4.32): in these layers the velocity U is opposite in sign to the velocity U of the fluid above the bottom.

5. The determination of the sheet flow thickness was fruitless because in the experiment the presence of a cloud of particles in suspension has led to incorrect calculation of the thickness of sheet flow.

6. The model of Sleath in this experiment did not lead to good results

for the estimation of shear stress. Possible causes are:

- to calculate the shear stress in the upper layer of the plug flow should be measured velocity U and V relating to the fluid and not related to the particles;
- because of the phase lag. When the pressure in the bed is greater than the pressure of the fluid there is dilation in the bed, so the vertical velocity V is positive and also is easier the formation of plug flow. In the same moment the velocity U is negative because we are in the trough and so the shear stress calculated by $\tau = -\rho\tilde{u}\tilde{v}$ is positive, but it was expected a negative value in agreement with the physical reality;
- perhaps there are other terms for forces in play that it isn't know or it wasn't considered the presence in the formulation of the model.

Bibliography

[1] Adrian R.J., (2005), *Twenty years of particle image velocimetry*. Experiments in Fluids (2005) 39: 159–169.

[2] Asano T., (1990), *Two-phase model on oscillatory sheet-flow*. Proceedings of the 22nd International Conference on Coastal Engineering, pp. 2372-2384, Am. Soc. of Civ. Eng., New York.

[3] Bagnold, R. A., (1946), *Motion of waves in shallow water, interaction between waves and sand bottoms*. Proc. R. Soc. London, Ser. A, 187(1008), 1–18.

[4] Bagnold, R. A., (1956), *The flow of cohesionless grains in fluids*. Phil. Trans. R. Soc. London, A, 249, 235-297.

[5] Berni C., Barthélemy E., Michallet H., (2013), *Surf zone cross-shore boundary layer velocity asymmetry and skewness: An experimental study on a mobile bed*. Journal of geophysical research: oceans, vol. 118, 1–13.

[6] Dick, J.E., Sleath, J.F.A., (1991), *Velocities and concentrations in oscillatory flow over beds of sediment*. Journal of Fluid Mechanics 233, 165-196.

[7] Dohmen-Janssen C. Marjolein, W. N. Hassan, J. S. Ribberink, (2001), *Mobile-bed effects in oscillatory sheet flow*. J. Geophys. Res., 106, 27,103– 27,115.

[8] Dohmen-Janssen C. Marjolein, Daniel M. Hanes, (2002), *Sheet flow dynamics under monochromatic nonbreaking waves*. Journal of geophysical research, vol. 107, no. C10, 3149.

[9] Dohmen-Janssen C. Marjolein, Daniel M. Hanes, J. S. Ribberink, (2002), *Phase-lags in oscillatory sheet flow*. Coast. Eng., 46, 61–87.

[10] Foster D. L., Bowen A. J., Holman R. A., Natoo P., (2006), *Field evidence of pressure gradient induced incipient motion*. Journal of geophysical research, vol. 111, c05004.

[11] Lu Louise, Sick Volker, (2013), *High-speed Particle Image Velocimetry Near Surface*. Journal of Visualized Experiments.

[12] Nielsen, P., (1992), *Coastal Bottom Boundary Layers and Sediment Transport*. World Scientific, Singapore.

[13] Rodrıguez-Abudo S., Foster D. L., Henriquez M., (2013), *Spatial variability of the wave bottom boundary layer over movable rippled beds*. Journal of geophysical research: oceans, vol. 118, 1–17.

[14] Rusello Peter J., Lohrmann Atle, Siegel Eric, Maddux Tim, (2006), *Improvements in acoustic doppler velocimetry*. The 7th Int. Conf. on Hydroscience and Engineering (ICHE-2006),Sep 10 –Sep 13,Philadelphia,USA.

[15] Sleath, J.F.A., (1994), *Sediment transport in oscillatory flow*. Sediment Transport Mechanisms in Coastal Environments and Rivers, M.

Belorgey, R.D. Rajaona, and J.F.A. Sleath, eds., World Scientific, Singapore.

[16] Sleath, J.F.A., (1994), *Sediment transport in oscillatory flow.* In: Belorgey, M., Rajaona, R.D., Sleath, J.F.A. (Eds.), Sediment Transport Mechanisms in Coastal Environments and Rivers. World Scientific, Singapore.

[17] Sleath, J.F.A., (1998), *Depth of erosion under storm conditions.* Proceedings of the 26th Conference Coastal Engineering ASCE, New York (in press).

[18] Sleath, J.F.A., (1999), *Conditions for plug formation in oscillatory flow.* Continental Shelf Research 19, 1643-1664.

[19] Sommeria Joel, (2003), *Correlation Imaging Velocimetry at the Coriolis facility.* `http://www.legi.grenoble-inp.fr/web/IMG/pdf/CIV_doc_lim.pdf`

[20] Zala Flores N., and Sleath J.F.A., (1998), *Mobile layer in oscillatory sheet flow.* J. Geophys. Res., 103, C6, 12 783-12 793.

Web site

http://www.jove.com/video/50559

http://www.lavision.fr/fr/techniques/piv.php

http://servforge.legi.grenoble-inp.fr/projects/soft-uvmat/wiki

http://servforge.legi.grenoble-inp.fr/projects/soft-uvmat/wiki/UvmatHelp

http://www.sontek.com/productsdetail.php?10-MHz-ADV-2

http://www.nortek-as.com/en/products/velocimeters/vector

http://www.nortek-as.com/en/products/velocimeters/vectrino-ii

http://www.nortek-as.com/en/products/current-profilers

http://www.nortek-as.com/en/products/velocimeters

http://www.visionresearch.com/

http://www.visionresearch.com/Products/High-Speed-Cameras/Miro-M310/

http://www.visionresearch.com/Solutions/Case-Studies/

http://www.visionresearch.com/Products/Accessories-Options/PCC-Software/

http://www.legi.grenoble-inp.fr/web/spip.php?article763

http://www.legi.grenoble-inp.fr/web/IMG/pdf/hydralab_YP_joel.pdf